Faktoren die der Frequenzresponce eines Lasers beeinflussen

a) Injektionsstrom und Schwellstrom

Aus der Übertragungsfunktion geht klar hervor, daß bei höherer Photonendichte $\bar{S}$ eine höhere Resonanzfrequenz erhalten wird

⇒ Ein niedriger Schwellstrom ist deshalb wichtig, da bei einem Laser mit niedrigem Schwellwert bei gleichem Injektionsstrom die Photonendichte (Ausgangsleistung) höher ist und damit auch die Resonanzfrequenz

b) Auger effekt

Der Auger effekt hat zwei wichtige Einflüsse.

- Reduzierung des für opt. Photonen zur Verfügung stehenden Stromanteils ⇒ $\bar{S}$ kleiner ⇒ ω_r kleiner
- Der Dämpfungsfaktor wird

$$\gamma(\text{Auger}) = \gamma(I_{Aug}=0) + \frac{1}{e}\cdot\frac{\partial J(\bar{n}_{2D})}{\partial n_{2D}}$$

⇒ der Dämpfungsfaktor wird größer und die Device responce bleibt?

c) Photonen lebensdauer

Für eine hohe Resonanzfrequenz sollte τ_{ph} so klein als möglich gemacht werden. Dies kann durch kürzere Resonatorlängen erreicht werden. Gleichzeitig wird dadurch jedoch der Anteil der Resonatorverluste erhöht sodaß ein höherer $n_{2D}(th)$ für den selben Gain notwendig ist.

⇒ optimale Resonatorlänge eines Lasers (typisch bei QW-Laser ~100µm)

Man muß jedoch beachten, daß die Photonenlebensdauer stark mit dem Gain und dem Schwellstrom gekoppelt ist ☹

d) Differentieller Gain:

In dem Ausdruck für die Resonanzfrequenz kommt als weitere Größe $\frac{\partial g(\bar{n}_{2D})}{\partial n_{2D}}$ vor die auch als "differentieller Gain" bezeichnet wird. Durch die Auswahl von Bauelementen mit großem differentiellen Gain in der aktiven Zone kann ebenfalls f_r erhöht werden. Dies kann zum Beispiel durch Verwenden von Quantum Well Strukturen und verspannten QW Strukturen, die einen höheren $\frac{\partial g}{\partial n_{2D}}$ haben erreicht werden.

⇒ lasen bis zu ~40 GHz erreicht

State of the Art QW-Laser arbeiten bis zu 35 GHz

Spektraler Output und Laser Linienbreite

Da eine der wichtigsten Anwendungen von Halbleiterlasern die optische Datenübertragung ist die Linienbreite des Ausgangsignals von entscheidender Bedeutung. Es ist entscheidend für die Anwendung von kohärenten Detektionsmöglichkeiten bei Verwendung von AM (Amplitudenmodulation) und FM (Frequenzmodulations) techniken (Phasenempfindliche Detektion). Hier kommt die Dispersion der Glasfaser ins Spiel die verschiedene Sichtfrequenzen unterschiedlich schnell überträgt. Die Linienbreite des Lasers ist deshalb ausschlaggebend welche Übertragungstechnik angewendet werden kann. Je schmäler die Linienbreite desto besser. ⇒ Folie Anforderung an die Linienbreite (Folie 178)

Faktoren die die Linienbreite kontrollieren sind in der nächsten Folie dargestellt

a) Güte des Optischen Resonators

b) Elektrischen Eigenschaften der aktiven Schicht
(Änderung des Brechungsindexes mit der e-h Zahl)

c) angewendete Modulationsverfahren

Anforderungen an die Linienbreite eines HL-Lasers für unterschiedliche Übertragungssysteme

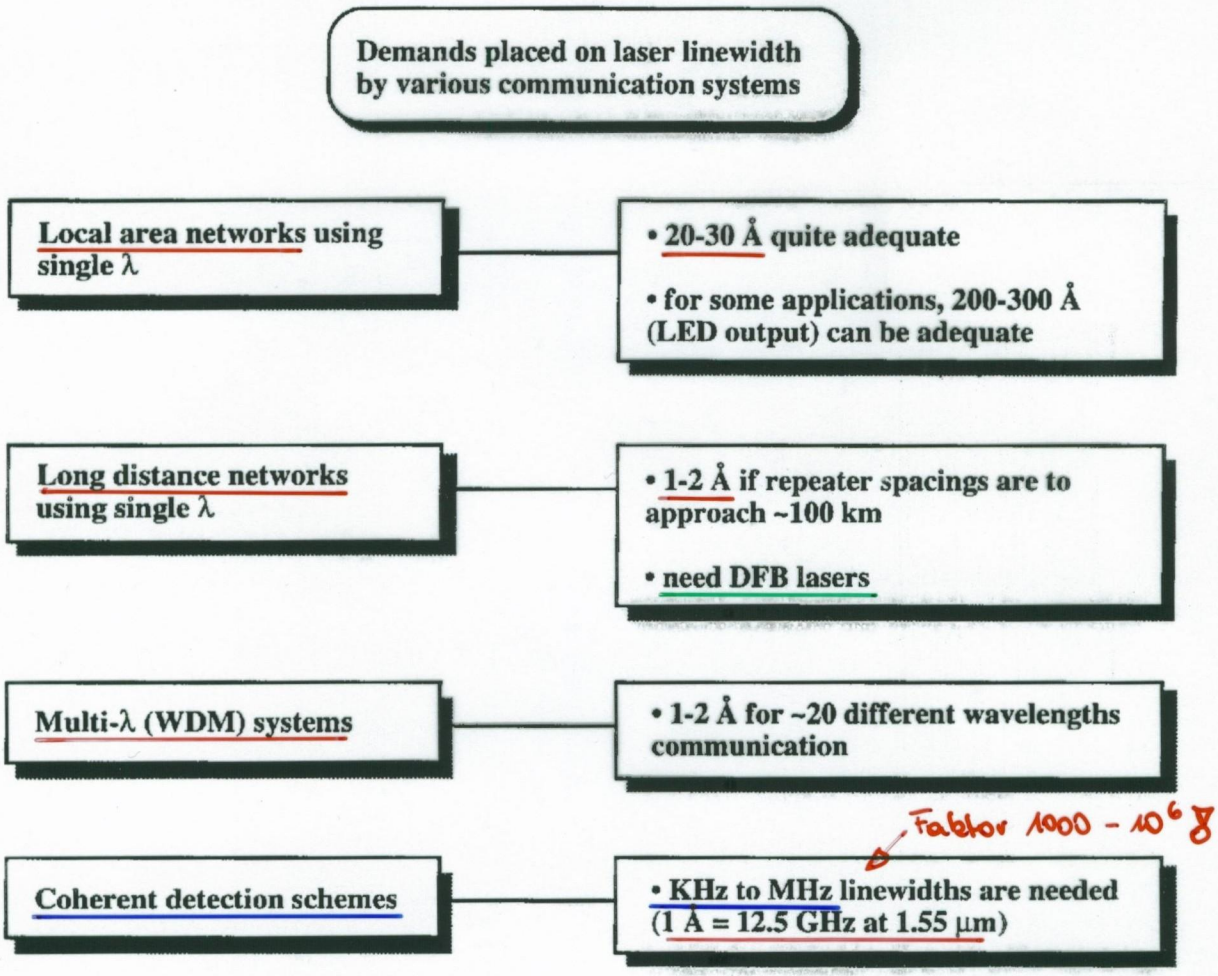

Figure 11.15: Important linewidth requirements for various optical communication schemes.

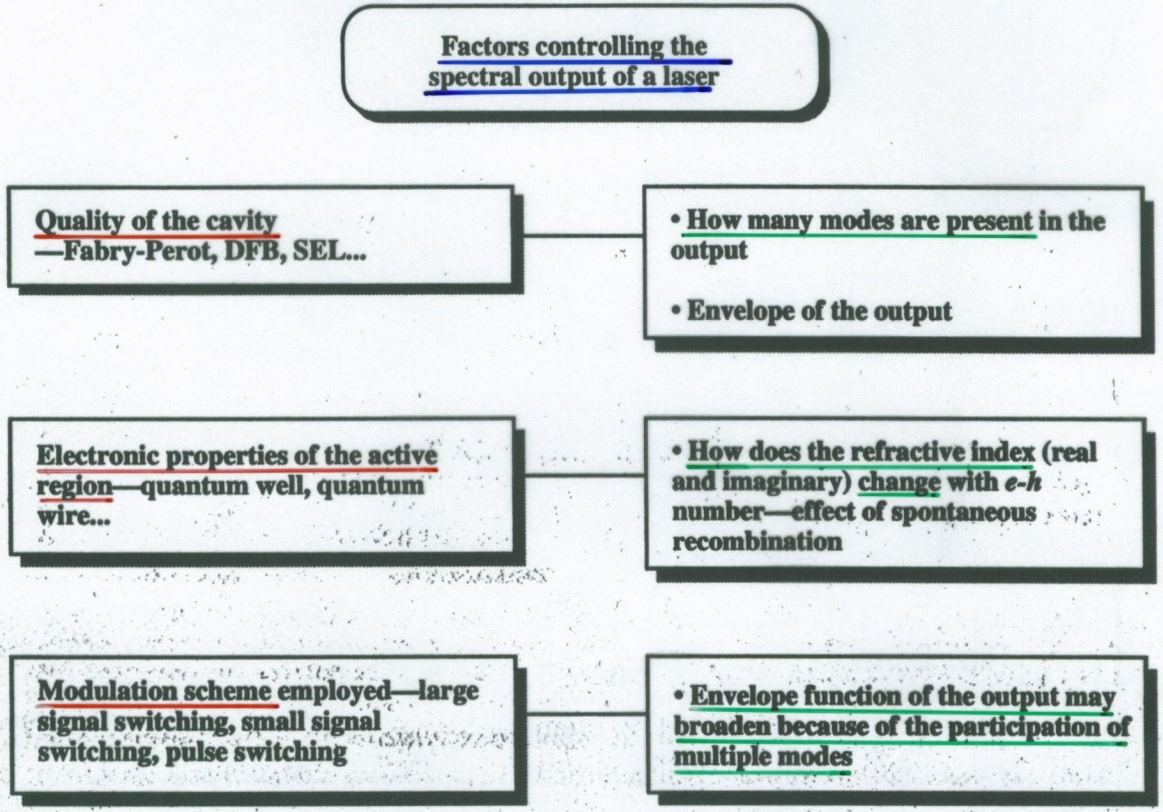

Figure 11.16: A list of important factors controling the linewidth of semiconductor laser output.

a) Optischer Resonator (Einfluss auf Linienbreite)

Der optische Resonator ist eine kritische Komponente des HL-Lasers da das Bauelement sonst als LED wirken würde.

1) Anzahl der Lasermoden des Ausgangssignals
2) Breite jeder Mode selbst.

Linienbreite einer einzelnen Mode des Laserausgangssignals:

Dies entspricht entweder einem DFB-Laser oder einem FP-Laser der bei hohen Injektionsströmen betrieben wird.

Die Breite des Transmissionsspektrums eines optischen Resonators ist durch ($\Delta\omega \cdot \Delta t \sim 1$, Unschärferelation) gegeben:

$$\Rightarrow \boxed{\Delta\omega \sim \frac{1}{\tau_{ph}} \simeq \frac{c \cdot |\ln R|}{n_r \cdot L}}$$

wobei τ_{ph} die Photonenlebensdauer im Resonator ist.

In Gaslaser ist die Resonatorlänge L sehr lang (einige m) sodass die Transmissionsresonanzen sehr scharf sind

In HL-Lasern sind jedoch die Resonatoren relativ kurz ($\sim 100\,\mu m - 1\,mm$) und die Transmissionsresonanzen sind deshalb im THz Bereich ($1\,Å \triangleq 12.5\,GHz \quad \Rightarrow \quad 1\,THz \triangleq 80\,Å$) (Faktor 10^7 in der Länge), und liefert deshalb keine Selektivität für enge Linienbreiten.

Die intrinsische Eigenschaft eines Resonator wird oft durch den Gütefaktor $\boxed{Q := \frac{\omega}{\Delta\omega}}$ beschrieben. Für HL-Laser ist dieser Faktor jedoch nicht sehr hoch, sodass die Linienbreite durch die optischen Prozesse die sich im HL ereignen bestimmt wird

b) Spontane Emission und Linienbreitenvergrößerungsfaktor

(Linewidth Enhancement Factor α_{enh})

Bei unserer Diskussion des Lasers haben wir zwei Emissionsprozesse diskutiert

a) spontane Emission (LED) ⇒ nicht kohärentes Licht

b) stimulierte Emission ⇒ kohärentes Licht (selbe Frequenz u. Phase)

Die Photonen die jetzt spontane Emittieren haben mit den anderen keine Kohärenz sodaß es intuitiv offensichtlich ist, daß sie eine wichtige Ursache für die Inkohärenz oder Linienbreite des Ausgangssignals sein werden.

Effekt der Ladungsträgerinjektion in der aktiven Zone:

Ladungsträgerinjektion beeinflußt sowohl den Realteil des Brechungsindexes als auch den Imaginärteil. Der Imaginärteil des Brechungsindexes hängt mit dem Absorptionskoeffizient bzw. mit der Verstärkung (Gain) zusammen, während der Realteil die Phasengeschwindigkeit des Lichts bestimmt (d.h. Umlaufzeit t_{ph})

Beide Teile hängen wiederum über die Kramers-Kronig Relation zusammen.

Sind $\Delta n_r'$ und $\Delta n_r''$ die Änderungen im Real- und Imaginärteil des Brechungsindexes, so ist

$$\Delta g = -\frac{2\omega}{c}\,\Delta n_r''$$

wobei Δg die Änderung des Gain aufgrund der Ladungsträgerinjektion ist.

Für kleine Änderungen liefert die Kramers-Kronig Relation

$$\Delta n_r'(E) = \frac{2}{\pi}\,P\int_0^\infty \frac{E'\,\Delta n_r''(E')}{E'^2 - E^2}\,dE'$$

wobei P der Hauptwert des Integrals ist

Typische Werte in Folie (182)

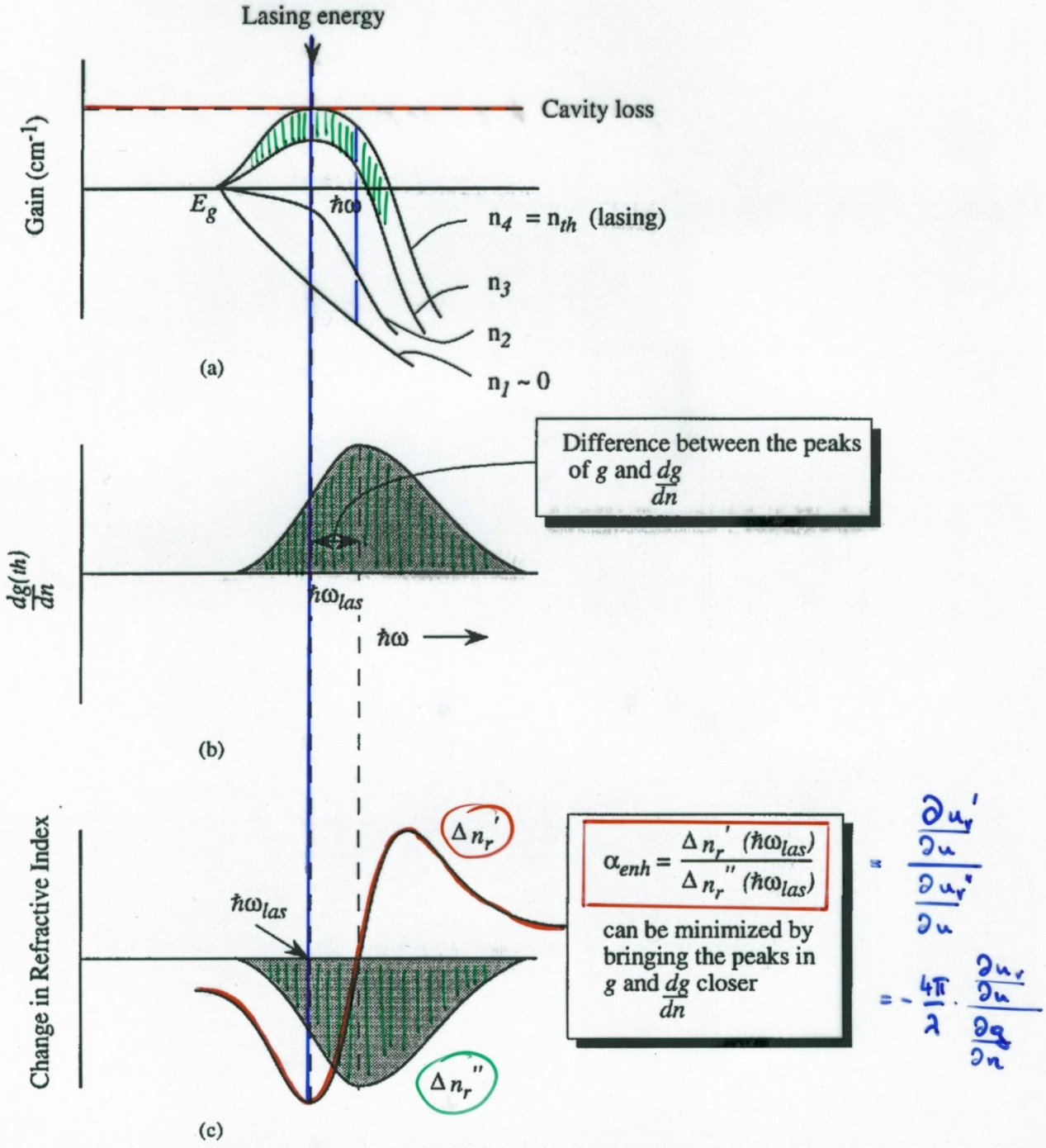

Figure 11.17: (a) The gain $g(\hbar\omega)$ of a semiconductor laser as a function of injection density. (b) The value of the change in the gain as the carrier density is changed. The changes in the real and imaginary part of the refractive index.

$$\frac{\partial n_r''}{\partial n} = -\frac{1}{2} \cdot \frac{dg}{dn} \cdot \frac{2\pi}{\lambda}$$

Die Änderung im Realteil des Brechungsindexes verursacht jetzt aber eine Verschiebung der lasermode und verbreitet deshalb die Emissionslänge. Ein wichtiger Parameter ist das Verhältnis der Änderung des Realteils des Brechungsindexes zum Imaginärteil des Brechungsindexes und dies wird als Linienbreitevergrößerungsfaktor $\alpha_{enh}(\hbar\omega_{las})$ bezeichnet.

$$\alpha_{enh} = \frac{\Delta n_r'(\hbar\omega_{las})}{\Delta n_r''(\hbar\omega_{las})} = \frac{\frac{dn_r'}{dn}}{\frac{dn_r''}{dn}} = -\frac{4\pi}{\lambda_{las}} \cdot \frac{\frac{dn_r'}{dn}}{\frac{dg}{dn}}$$

Dieser Faktor spielt eine wichtige Rolle in der Spektralen Breite einer einzelnen lasermode.

Wichtig ist wie aus Folie 182 ersichtlich, daß das Energie-Maximum in der Gainkurve meistens nicht mit dem Maximum der Kurve $\frac{dg}{dn}$ übereinstimmt.

Der Wert $\Delta n_r'$ wird bei dem Maximum der Kurve $\frac{dg}{dn}$ null. Aus diesem Grund wird α_{enh} niedrig bei dem Punkt wo $\frac{dg}{dn}$ maximal wird.

Eine Verringerung von $\alpha_{enh}(\hbar\omega_{las})$ erfordert deshalb die Wahl einer Struktur bei der das Gainmaximum mit dem Maximum von $\frac{dg}{dn}$ übereinstimmt.

Die spontane Emission die in lasern neben der stimulierten Emission auftritt verursacht eine Fluktuation der Phase und Amplitude des optischen Feldes und hat einen wichtigen Einfluß auf die Kohärent oder Linienbreite des lasersignals.

(siehe Folie S 184)

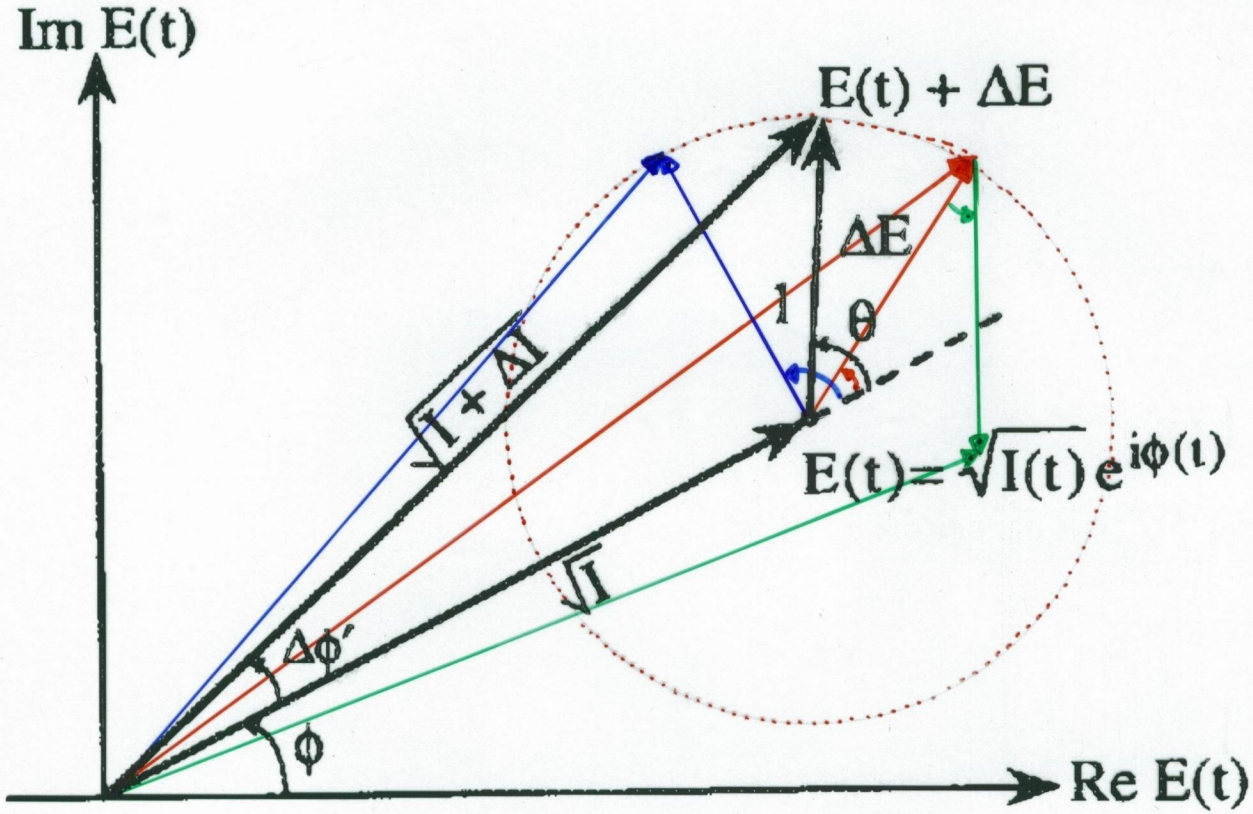

Figure 11.5. A plot on the complex optical electric field [29] $E(t) = \sqrt{I(t)}\exp[i\phi(t)]$ domain showing that its magnitude $\sqrt{I}$ and phase ϕ can be changed by the spontaneous emission of a photon (magnitude is one since the intensity I has been normalized to represent the photon number in the cavity) with a phase change $\Delta\phi'$.

Kit

$$F = \sqrt{P_0} \cdot \exp(-i\phi) \cdot \exp(i\omega_0 t)$$

P_0... Ausgangsleistung (Mittelwert)
ϕ... momentane Phase des Feldes
ω_0... Frequenz der Lasermode

Es gibt jetzt zwei Beiträge für die Phasenänderung:

a) $\Delta\phi'$ aufgrund einer 'Out-of-phase' Komponente von ΔF

b) $\Delta\phi''$ aufgrund einer Intensitätsänderung die mit einer Phasenänderung gekoppelt ist

Die spontane Emission addiert jetzt einen Photon beliebiger Phase wie in der Folie. Zusätzlich muß jetzt berücksichtigt werden, daß pro Zeiteinheit mehrere Photonen mit unterschiedlicher Phase in die Lasermode beitragen

(⇒ Random - Walk - Problem)

⇒ Resultat: **Linien breite**

$$\Delta f = \frac{(1 + \alpha_{enh}^2)}{4\pi \cdot S} \cdot \beta \cdot R_{sp}$$

S... # der Photonen
β... spontaner Emissionsfaktor
R_{sp}... spontane Rekombinationsrate
α_{enh}... linien breiten vergrößerungs faktor (tritt nur in HL auf)

Da $P_0 = \frac{1}{2} \cdot S \cdot \hbar\omega \cdot v \cdot \alpha_m$

$\hbar\omega$... totale Photonenenergie
$v \alpha_m$... escape
$v = \frac{c}{n_{gr}} = \frac{c}{(n + \omega \frac{dn}{d\omega})}$

$\alpha_m = \frac{1}{L} \cdot \ln \frac{1}{R}$ ... Spiegelverluste

$$\Delta f = \hbar\omega \cdot \frac{c}{n_{gr}} \cdot \frac{\ln(1/R)}{L} \cdot \frac{1}{8\pi} \cdot \frac{R_{sp}}{P_0} \cdot (1 + \alpha_e^2)$$

$P = A \cdot \frac{S \hbar\omega}{\tau_{ph}}$

$\frac{1}{\tau_{ph}} \sim \frac{c}{n_{gr}} \cdot \frac{|\ln R|}{L}$

$$\Delta f \sim \frac{1}{P_0}$$

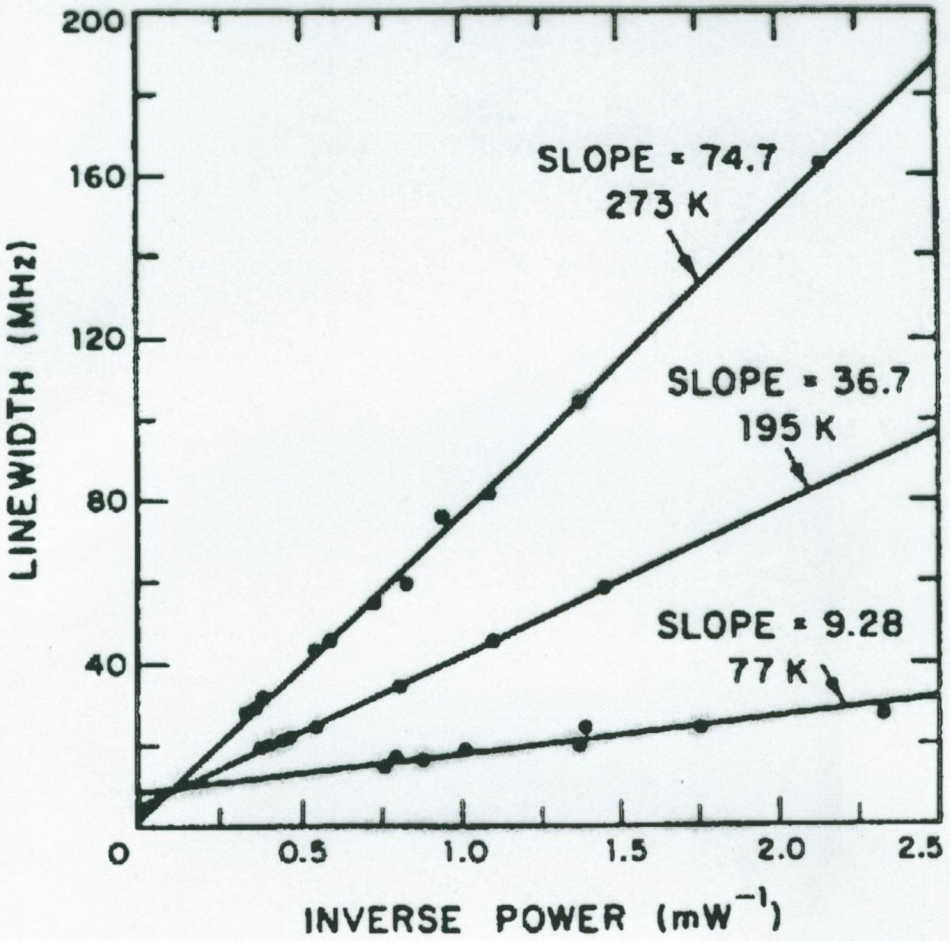

Figure 11.6. Semiconductor laser linewidth versus inverse power at three temperatures exhibiting the linear behavior. (After Ref. 33.) The magnitude of the large linewidth was explained [29] using the correction factor $1 + \alpha_e^2$ with $\alpha_e \simeq 5$ at room temperature.

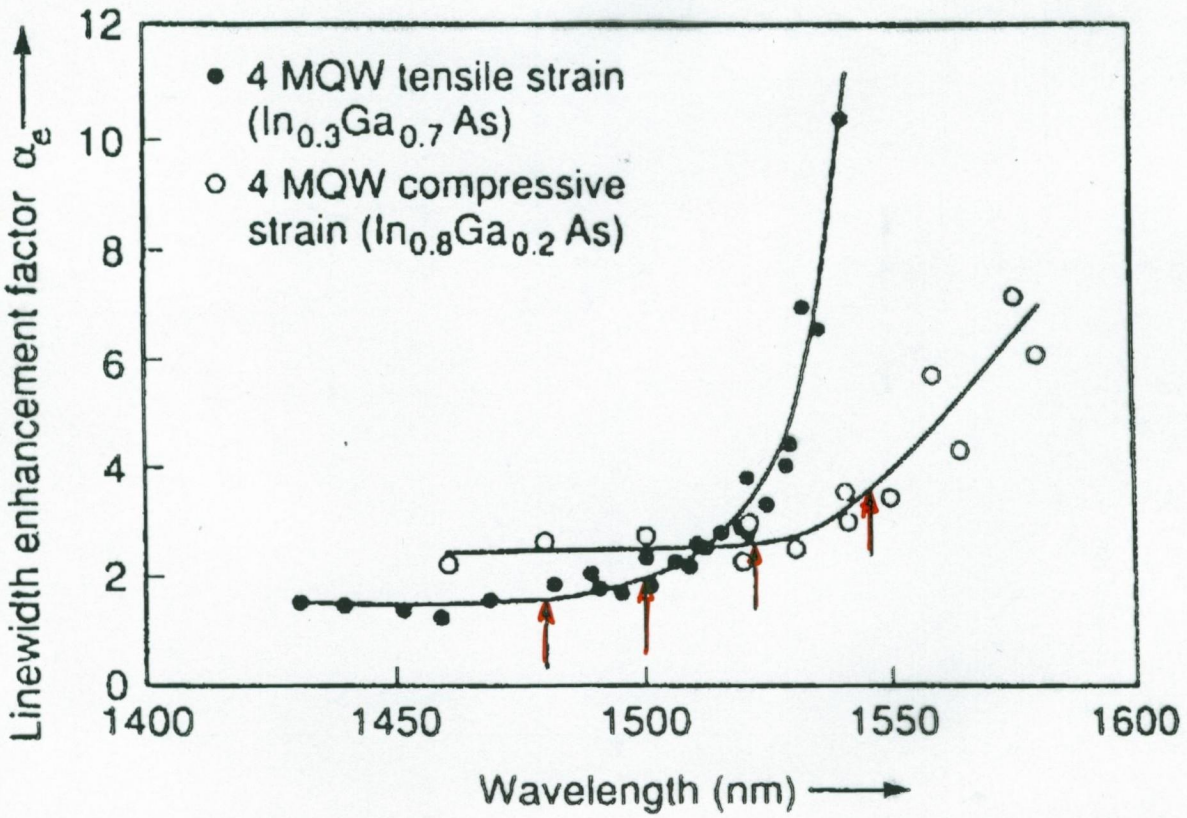

Figure 11.7. The linewidth enhancement factor α_e vs. wavelength of two types of strained MQW lasers. The lasing wavelength is indicated by the arrows. (After Ref. 14.)

c) Laserspektren unter Modulationsbedingung

Wird ein Laser moduliert, dann tendiert das Ausgangsspektrum eines Lasers zur Verbreiterung. Die Größe der Verbreiterung hängt von der Art der Modulation ab, die verwendet wird.

Bei FP-Lasern können dadurch mehrere Moden angeregt werden

⇒ siehe Folie Seite 188

Bei einmodigen Lasern (z.B. DFB-Lasern) tritt der sogenannte "Chirp" oder "Frequenzchirp" unter Modulation auf. Dies ist eine Verbreiterung aufgrund der Ladungsträgeränderung und der nicht linearen Response des Lasers

für Puls code Modulation

$$\Delta\nu_{chirp} = \frac{1}{2\pi}\frac{d\phi}{dt} = \frac{c}{n\nu}\cdot\frac{\alpha_{em}}{4\pi}\left(\Gamma g - \alpha_c\right) = \frac{1}{4\pi}\,\alpha_{em}\cdot v\cdot(\Gamma g - \alpha_c)$$

$$= \frac{\beta c}{4\pi}\cdot\frac{I_{mod}}{e}\cdot\frac{1}{G\cdot P_0}\cdot\sqrt{\omega_m^2 + \tau_p^{-2}}$$

für sinusförm. Modulat

$$G \approx \frac{1}{\tau_{ph}} = \frac{c}{n_i}\cdot\frac{|ln R|}{L}$$

mod. Frequenz

$$\Gamma_p = \frac{P_{sp}}{P_0} + \frac{G_L}{2}\cdot\frac{P}{(1+p)^{3/2}}$$

$$\Delta P\cdot\Gamma_p = \beta P_{sp}$$

$$v_g\cdot\alpha_m\cdot\tau_{ph}$$

$$\eta_d = \eta_i\,(v_g\cdot\alpha_m\cdot\tau_{ph}) = \eta_i\,\frac{\alpha_m}{\alpha_m+\alpha_{int}}$$

$$P_{out} = \frac{h\nu}{2}\cdot\eta_i\,(\quad)\,\frac{(I-I_{th})}{q}$$

$$\eta_d = \frac{2q}{h\nu}\cdot\frac{dP_{out}}{dI}$$

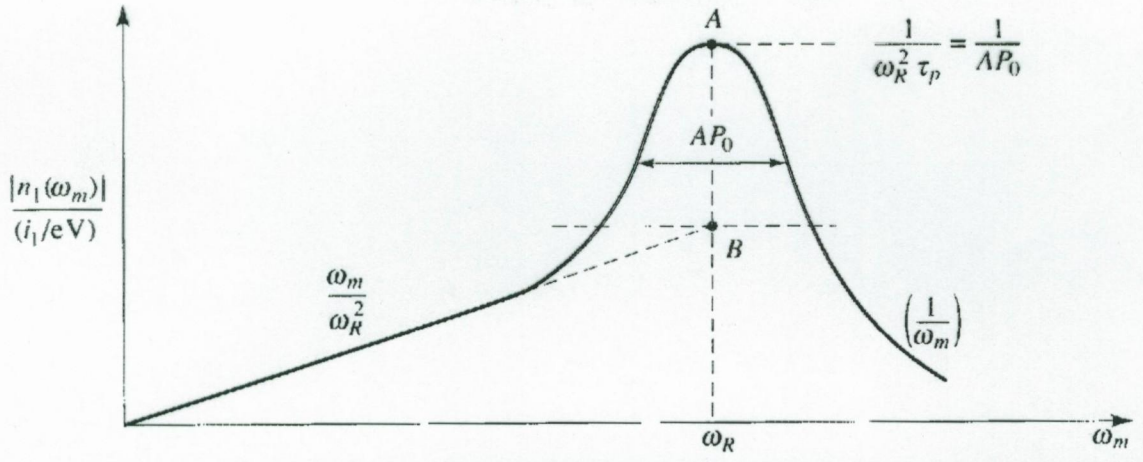

(a)

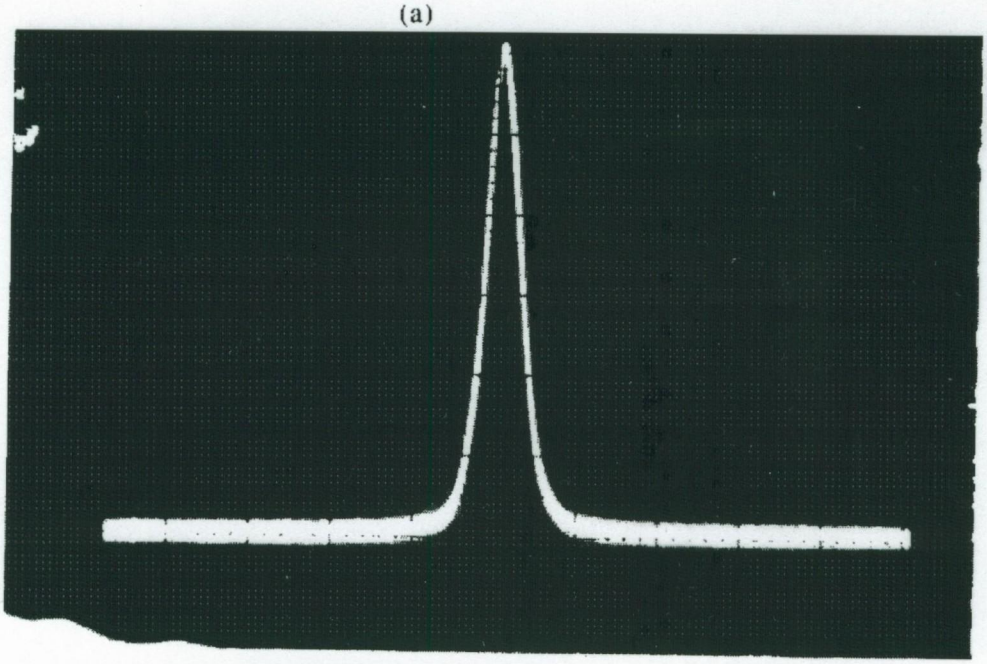

FP-laser nicht moduliert

(1)

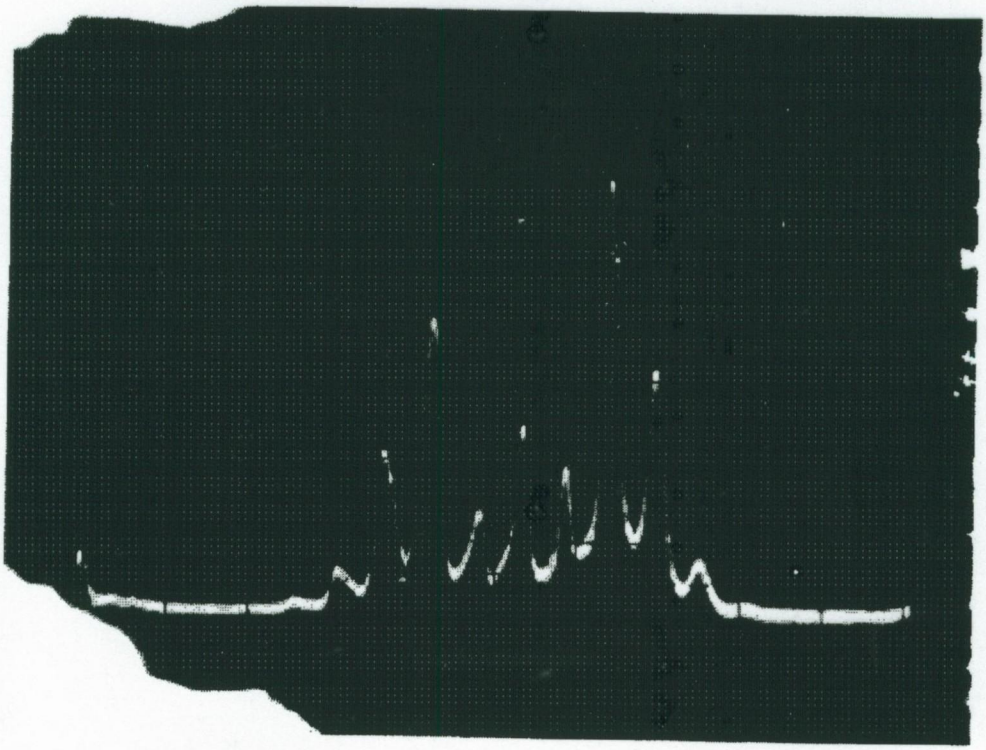

FP-laser moduliert

(2)

Figure 15-20 (a) A theoretical plot of the carrier density modulation n_1 as a function of the current modulation frequency ω_m. (b) (1) A scanning Fabry–Perot spectrum of a GaInAsP (λ = 1.31 μm) DFB laser with no current modulation. (2) The spectrum of the same laser when the current is modulated at f_m = 550 MHz, horiz. scale = 1 GHz/div. (Courtesy of H. Blauvelt, P. C. Chen, and N. Kwong of ORTEL Corporation, Alhambra, California)

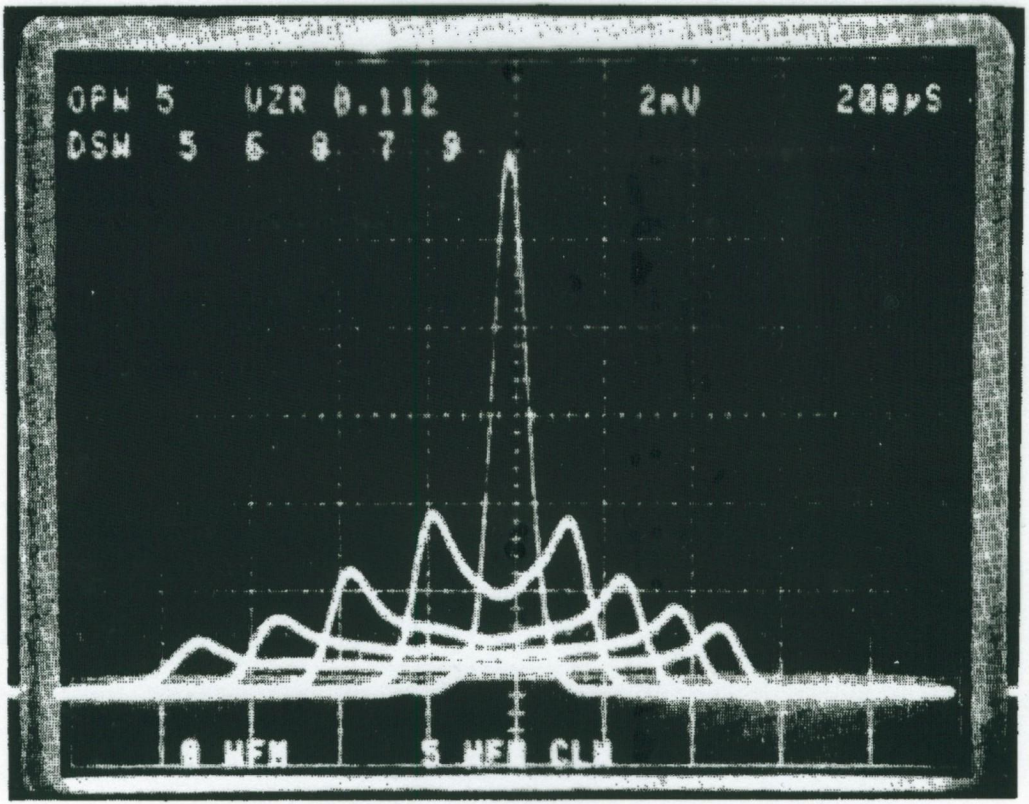

Fig. 6.19 Time-averaged power spectra of a 1.3-μm InGaAsP laser under sinusoidal modulation at 100 MHz. Spectrum broadens with an increase in the modulation current due to frequency chirping. The horizontal scale is 0.5 Å per division. (After Ref. 116)

Zusammenfassung

TOPICS STUDIED	KEY OBSERVATIONS
Large signal switching of a laser	When a laser is switched from below threshold to above threshold, there is a time delay in the photon output followed by relaxation oscillations. Up to 10 ns elapse before the photon output stabilizes.
Small signal modulation of a laser	Small signal modulation can have cutoff frequencies as high as 40 GHz. The response is improved by biasing the device at high power, using a low threshold device and using a material with high differential gain.
Gain compression effects	At very large biasing, the fast *e-h* recombination at the lasing mode causes a hole to burn in the distribution function. This reduces the gain of the device and affects the small signal modulation response.
Pulse code modulation of lasers	The laser output is not very faithful to the input signal. The output spectra can be broadened and the output frequency limits are lower than the small signal limits.
Extrinsic effects on laser modulation	• For high speed modulation, a laser has to be biased at a very high photon density. Heating and damage limit how high this bias point can be. • Parasitics have to be carefully reduced for high speed lasers.
Linewidth of lasers	• In multimode lasers (Fabry-Perot), the laser linewidth is controlled by the envelope function of the output. The linewidth is ~10Å in such lasers. • In single mode lasers (DFB), the linewidth is controlled by phase and intensity fluctuations due to spontaneous emission. Linewidth of a few MHz can be achieved without any external cavities.

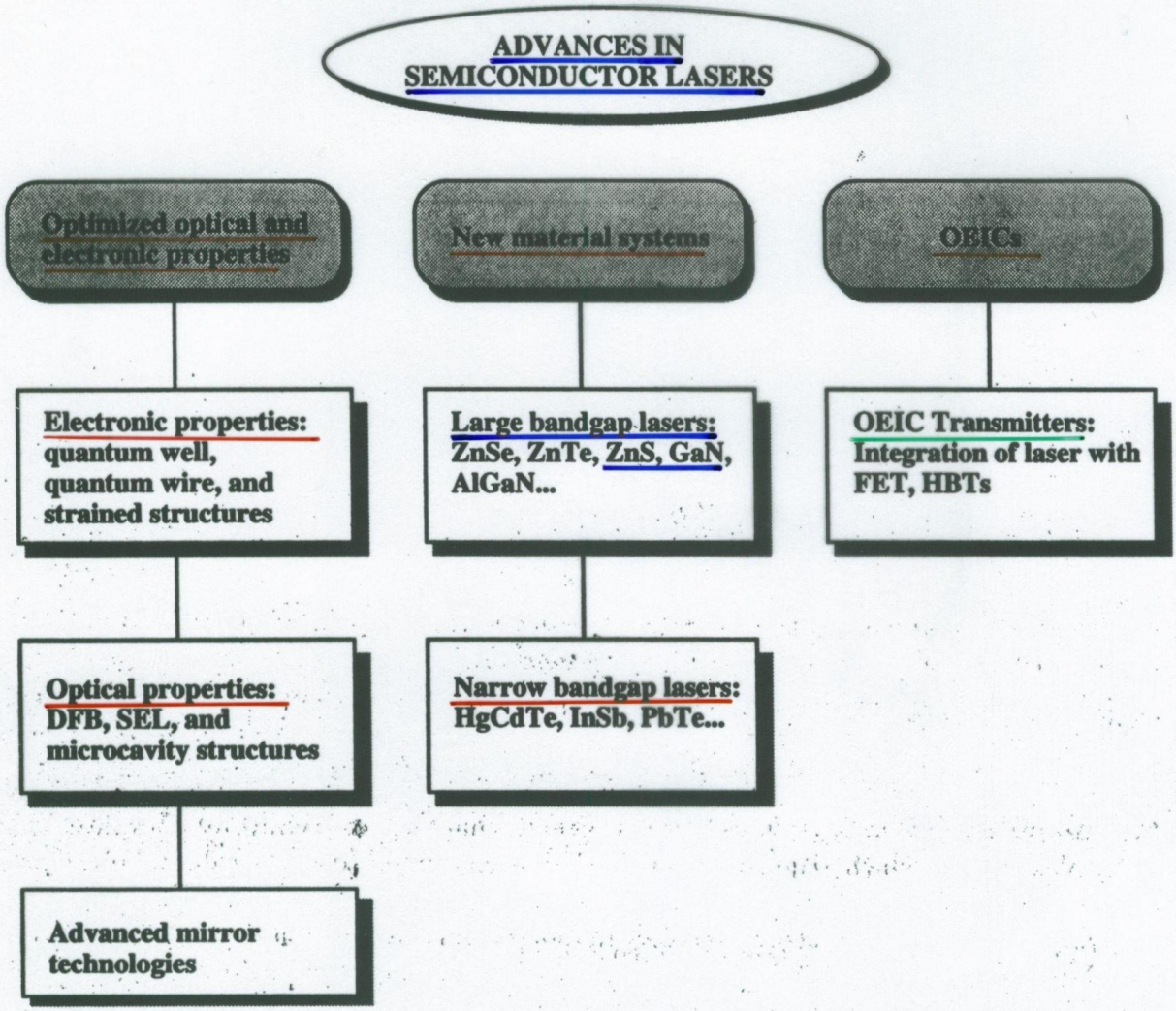

Figure 11.19: Advances in laser technology are being driven by the motivations outlined in this figure.

OEIC -- optoelectronic integrated circuits

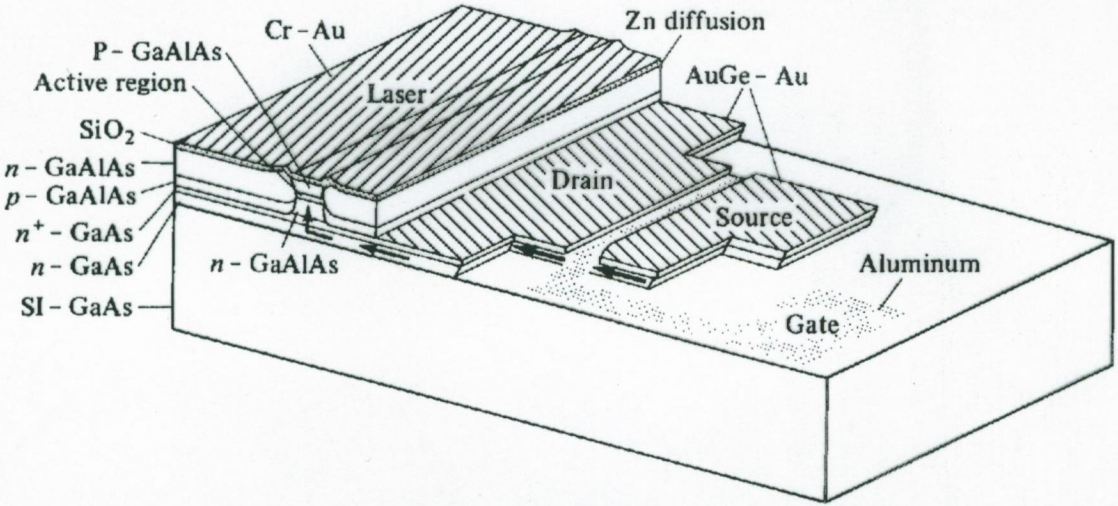

Figure 15-21 A GaAs n-channel field-effect transistor integrated monolithically with a buried heterostructure GaAs/GaAlAs laser. The application of a gate voltage is used to control the bias current of the laser. This voltage can oscillate and modulate the light at frequencies > 10 GHz. (After Reference [31].)

d.h. Laser + Lasertreiber

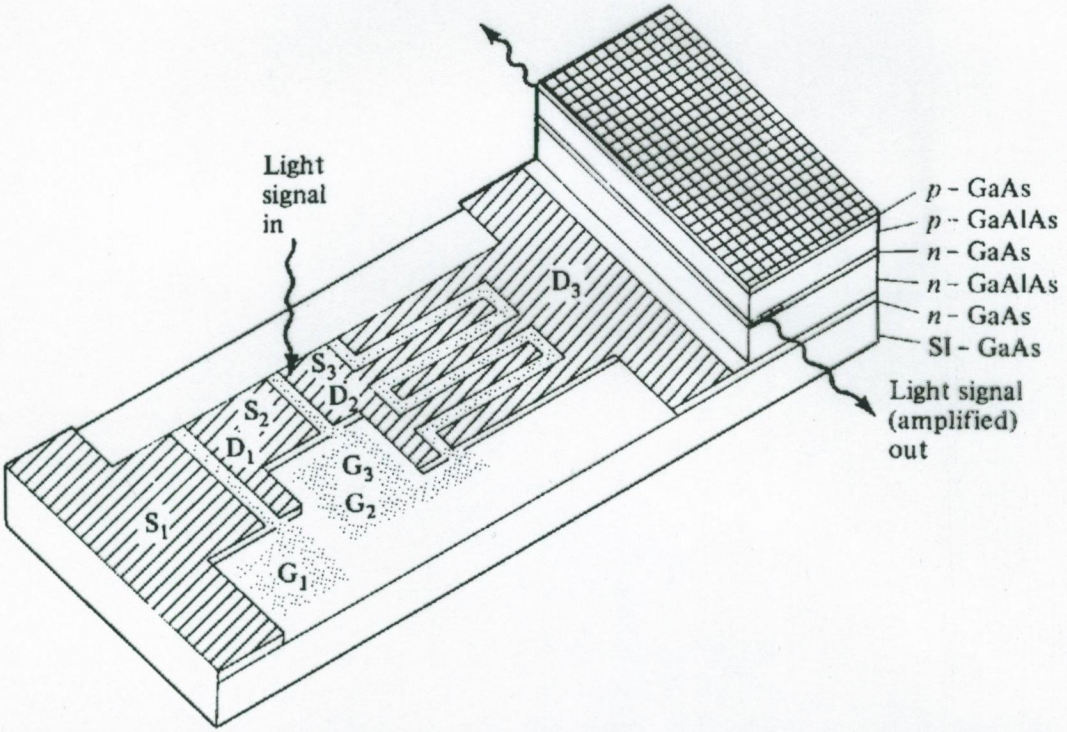

Figure 15-22 A monolithically integrated optoelectronic repeater containing a detector, transistor current source, a FET amplifier, and a laser on a single crystal GaAs substrate. (After Reference [32].)

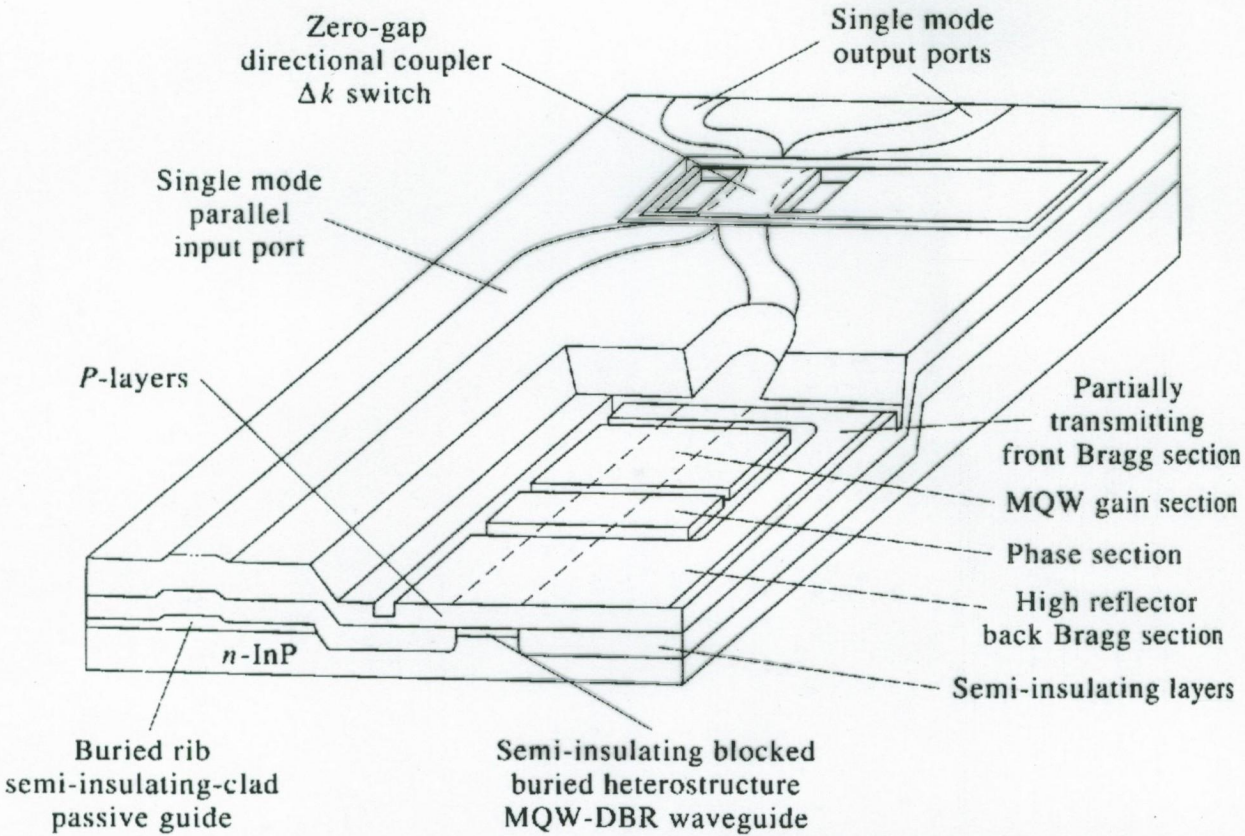

Figure 15-23 A monolithic circuit containing a tunable multisection InGaAsP/InP 1.55 μm laser employing multiquantum well gain section, a passive waveguide for an external input optical wave, and a directional coupler switch for combining the laser output field and that of the external input at the output ports. (After Reference [34].)

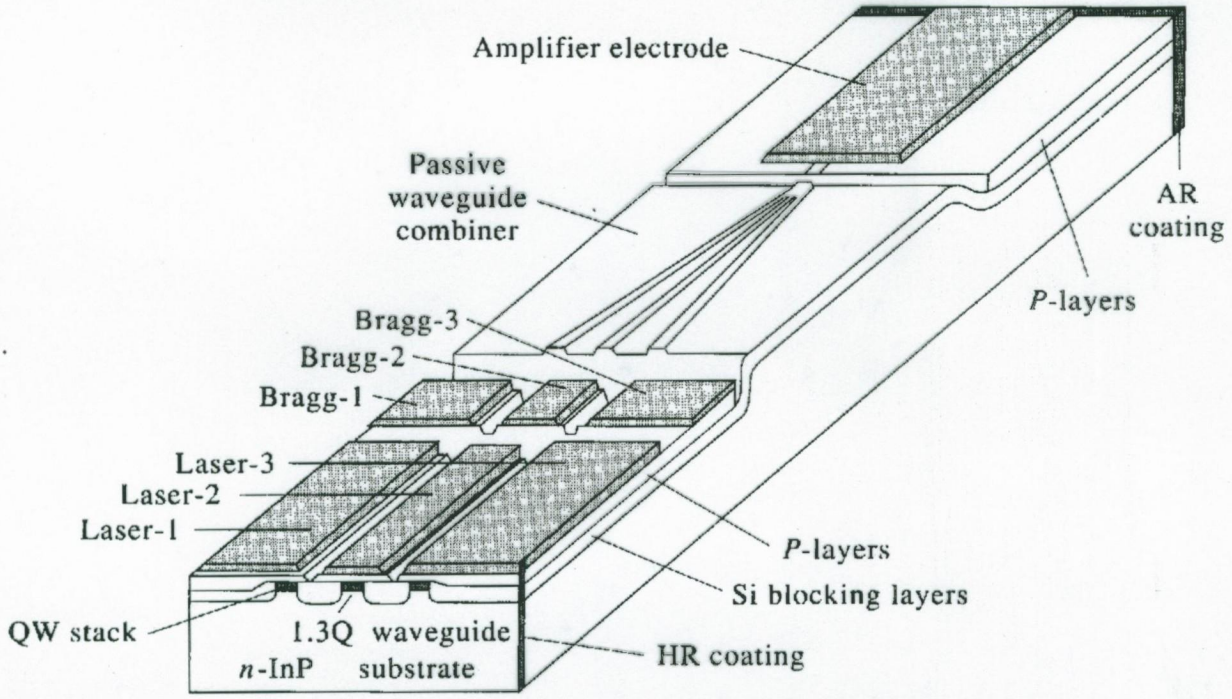

Figure 15-24 An optoelectronic integrated circuit composed of three ~1.5 μm InGaAs/InP distributed feedback lasers each tuned to a slightly different wavelength. The three wavelengths are fed into a single waveguide and amplified in a single amplifying section. (After Reference [35].)

Optoelektronische Detektoren

Eine der wichtigsten Aufgaben bei der Informationsübermittlung ist neben der Sendequellen (Laser) die Detektion der Information. Hier werden wir jetzt die wichtigsten Eigenschaften und Arten von optischen Detektoren kennen lernen.

1.) Optische Absorption in Halbleitern

Der photonen absorptions prozess ist am stärksten in einem Halbleiter mit direkter Bandlücke wo die Impulserhaltung kein zusätzliches Phonon benötigt und ein Elektronen-Loch-Übergang der vertikal im k-Raum ist erfolgt.

Für solche Halbleiter kann der Absorptionskoeffizient geschrieben werden als

$$\alpha(\hbar\omega) = \frac{2\pi \cdot e^2 \hbar}{3 \cdot \mu_r \cdot c \cdot m_0^2 \cdot \varepsilon_0} \cdot \frac{|P_{cv}|^2}{\hbar\omega} \cdot \frac{\sqrt{2} \cdot (m_r^*)^{3/2} \cdot (\hbar\omega - E_g)^{1/2}}{\pi^2 \cdot \hbar^3}$$

bzw:

$$\alpha(\hbar\omega) \approx 4 \cdot 10^6 \cdot \left(\frac{m_r^*}{m_0}\right)^{3/2} \cdot \frac{(\hbar\omega - E_g)^{1/2}}{\hbar\omega} \quad [cm^{-1}]$$

Für indirekte Halbleiter ist ein vertikaler Übergang im k-Raum nicht möglich und Elektronen können nur dann ein Photon absorbieren, wenn ein Phonon am Prozess teilnimmt. Diese Prozesse sind jedoch nicht stark und der Absorptionskoeffizient kann dann durch folgende Form beschrieben werden

$$\alpha_{indirekt} = (K_0 + K_1(T)) \cdot (\hbar\omega - E_g)^2$$

wobei K_0 eine Konstante und $K_1(T)$ ein temperaturabhängiger Faktor ist, der mit zunehmender Temperatur größer wird. Bei indirekten HL ist α typischer Weise einen Faktor 100 niedrigen (z.B. Si vs. GaAs)

Wie aus dem Ausdruck für α zu entnehmen ist, ist α nahezu 0 für Wellenlängen größer als die sogenannte

"Cut off - Wellenlänge" $\lambda_c = \frac{hc}{E_g} = \frac{1.24}{E_g(eV)}$ [μm]

Wichtig für einen Detektor ist, daß das Licht auch absorbiert werden kann, deshalb muß der Detektor eine entsprechende Dicke besitzen

Ist L die Probendicke, dann ist der Teil des absorbierten Lichts in der Probe

$$1 - \exp(-\alpha L)$$

sodaß für starke Absorption folgendes gelten muß

$$L > \frac{1}{\alpha(\hbar\omega)}$$

Für ein Licht mit ca 1.50eV benötigt man jetzt für

a) GaAs ~ 0.1 μm
b) Ge ~ 1 μm
c) Si ~ 10..20 μm

dicke Schichten

Ist der Absorptionskoeffizient eines HL-materials bekannt, dann benötigt man noch die Erzeugungsrate der e-h Paare

Fällt ein optischer Strahl der Intensität $P_{op}(0)$ auf einen HL pro Einheitsfläche, so ist die Intensität in der Tiefe x gegeben durch (Intensität hat Einheit W/cm²)

$$P_{op}(x) = P_{op}(0) \cdot \exp(-\alpha x)$$

Die Energie die pro Einheitsfläche und pro Sekunde in einem Dickenbereich der Dicke dx zwischen den Punkten x und $x+dx$ absorbiert wird ist

$$P_{op}(x+dx) - P_{op}(x) = P_{op}(0) \cdot [\exp(-\alpha(x+dx)) - \exp(-\alpha(x))$$

$$= P_{op}(0) \cdot [\exp(-\alpha x)] \cdot \alpha\, dx$$

erzeugt diese absorbierte Energie Photonen der Energie $h\nu$ so ist die Erzeugungsrate G_L (Rate pro Einheitsvolumen)

$$G_L(x) = \frac{\alpha \cdot P_{op}(x)}{h\nu} = \alpha\, f_{ph}(x)$$

wobei $f_{ph}(x)$ die Photonenflußdichte einfallend am Ort x ist (Fluß hat die Dimensionen $cm^{-2} s^{-1}$)

Sobald Licht auf einen HL fällt und dort e-h Paare erzeugt, dann hängt die Detektor-Performance von der Sammlung der Ladungsträger und damit einer Änderung der Leitfähigkeit eines Materials oder der Erzeugung eines Spannungssignals ab.

Bei Abwesenheit eines elektrischen Feldes oder Konzentrationsgradienten wird kein detektierbares Signal erzeugt sondern die e-h Paare rekombinieren wieder. Eine wichtige Eigenschaft eines Detektors wird durch die Stromempfindlichkeit (responsivity) R_{ph} beschrieben, die den erzeugten Strom bei einer bestimmten optischen Leistung angibt.

$$R_{ph} := \frac{I_L/A}{P_{op}} = \frac{J_L}{P_{op}}$$

"responsivity"

wobei I_L der erzeugte Photostrom in einem Bauelement der Fläche A ist und J_L die Photostromdichte

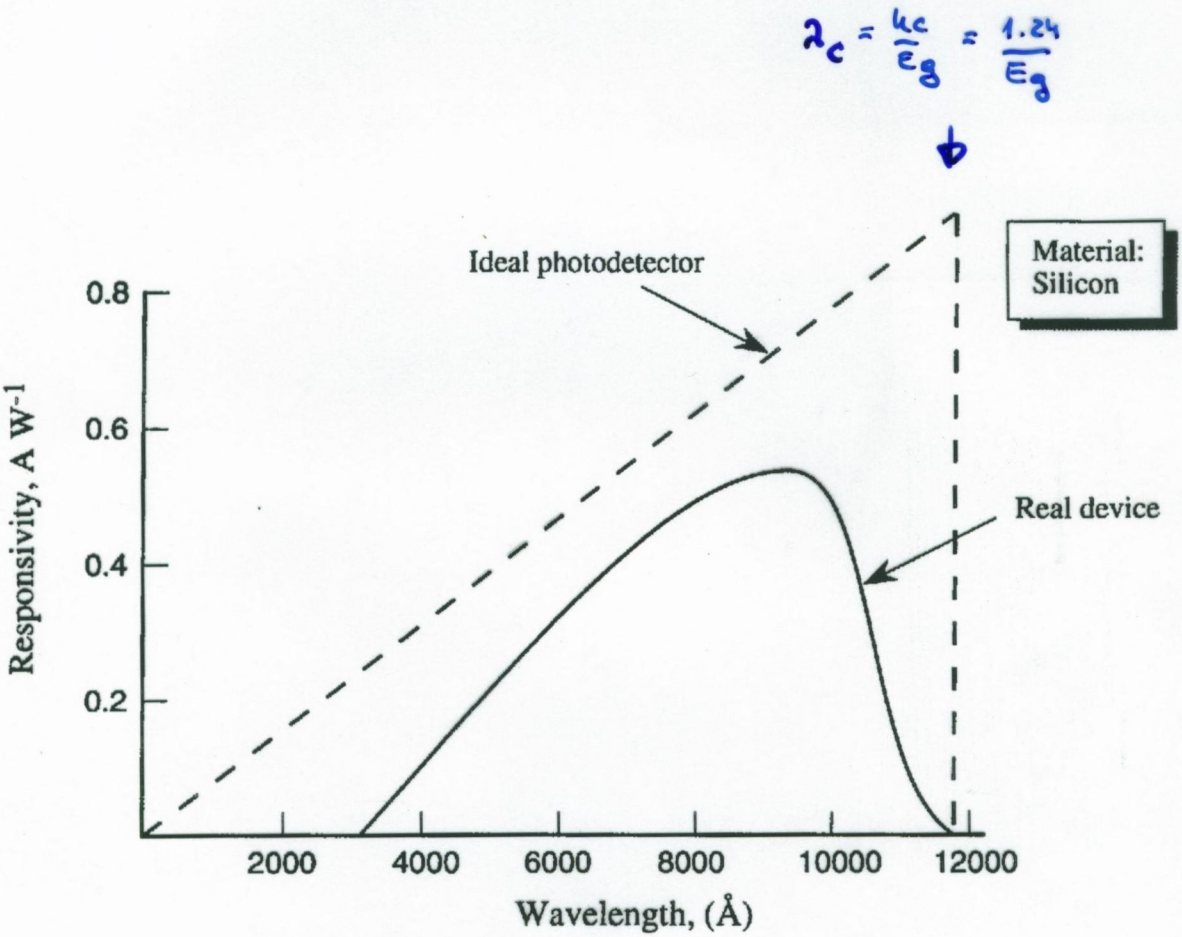

Figure 7.5: The responsivity curve of an ideal detector.

Die Quanteneffizienz eines Detektors η_Q wird durch

$$\eta_Q = \frac{I_{L/e}}{P_{op}/\hbar\omega} = R_{ph} \cdot \frac{\hbar\omega}{e}$$

definiert. Sie sagt uns wie viele Ladungsträger von jedem einfallenden Photon gesammelt wird. Die Erhöhung der η_Q ist deshalb eine der wichtigsten Aufgaben.

Die Stromempfindlichkeit eines Detektors hängt stark von der Wellenlänge des einfallenden Lichtes ab.

⇒ Folie Fig. 7.5

2) Rauschen und Detektionslimit

Um die Güte eines Detektors beurteilen zu können wurden mehrere Kenngrößen (Figure of merit parameters) entwickelt. Einer der wichtigsten Parameter ist dabei das schwächste (dc) Strahlungssignal welches noch detektiert werden kann. Dazu muß jedoch das Rauschen eines Detektors diskutiert werden.

a) Schrotrauschen (Shot Noise)

Die Elektronen (bzw. Photonen) die auf das stromerzeugende Bauelement fallen sind diskrete Teilchen deren Anzahl statistisch fluktuieren. Unter der Annahme, daß die Anzahl der Elektronenzahl im Zeitintervall σt Poissonverteilt ist, ergibt sich wenn a σt die mittlere Anzahl der Teilchen welche im Zeitintervall σt passieren folgende Verteilung

$$P(N, \Delta t) = \frac{1}{\sqrt{2\pi (a\Delta t)}} \exp\left(-\frac{(N - a\Delta t)^2}{2a\Delta t}\right) = \frac{1}{\sqrt{2\pi \bar{N}}} \exp\left(-\frac{\Delta N^2}{2\bar{N}}\right)$$

wobei $\bar{N} = a \cdot \Delta t$ der Mittelwert ist und
ΔN die Fluktuation um den Mittelwert

Die Funktion ist Maximal wenn $N = \bar{N} = a \cdot \Delta t$ ist

Die RMS (Root mean square) Abweichung der Poisonverteilung,
d.h. das Rauschen ist von der Statistik gegeben durch

$$\sqrt{(\overline{\Delta N})^2} = \sqrt{\overline{(N - \bar{N})^2}} = \sqrt{\bar{N}}$$

Das gemittelte Signal ist durch $\bar{N}$ $(= a \cdot \Delta t)$ gegeben

Damit folgt ein wichtiger Bauelementparameter, nämlich das

Signal zu Rausch-Verhältnis (SNR) für Schottrauschen

begrenzte Detektoren:

$$SNR = \frac{\bar{N}}{\sqrt{\bar{N}}} = \sqrt{\bar{N}} = \sqrt{a \cdot \Delta t}$$

fließt durch das Bauelement der Strom I so wird
die Teilchenstrom $a = \frac{I}{e}$ Außerdem wird das SNR umso
besser je länger das Beobachtungszeitintervall Δt ist. Für die
Bandbreite Δf eines Detektors gilt, daß

$$\Delta f \simeq \frac{1}{2 \cdot \Delta t}$$

$$\Rightarrow SNR = \sqrt{\frac{a}{2\Delta f}} \qquad \Rightarrow \text{bei hohen Frequenzen sinkt SNR-Verhältn}$$

Schottrauschenstrom:

$$\Rightarrow \left\{ I_{sh} = e \frac{\sqrt{\overline{\Delta N^2}}}{\Delta t} = \frac{e\sqrt{a \cdot \Delta t}}{\Delta t} = \sqrt{2 e I \Delta f} \right\}$$

Neben dem Schrottrauschen gibt natürlich viele andere Rauschmechanismen. Einer der wichtigeren ist das Rauschen aufgrund

b) thermischen Hintergrunds (Schwarzkörperstrahlung) die besonders bei IR-Detektoren berücksichtigt werden muß.

c) Thermisches Widerstandsrauschen $\overline{i^2_{Wth}} = 4 k_B T \cdot \Delta f / R$

d) Generations-Rekombinationsrauschen $\overline{i^2_{rg}} = 2 \cdot q \cdot G \cdot \frac{G \cdot \Delta f}{1 + (\omega \tau_g)^2}$

τ_g Lebensdauer

$$N(\lambda) = \frac{2c}{\lambda^4 \left[\exp\left(\frac{h\omega}{k_B T}\right) - 1\right]}$$

$\#/s$ / cm^2 · μm Wellenlänge

für $h\omega \ll E_g$ meist vernachlässigbar für fast alle opt.

Eine wichtige Kenngröße eines Detektors ist das geringste detektierbare Signal, welches denselben rms output wie das Rauschen erzeugt. Dies wird als äquivalente Rauschleistung NEP (noise equivalent power) bezeichnet.

Für den Fall wo der Detektor durch das Schrottrauschen limitiert ist, ist die optische Leistung die einen Photostrom I_L erzeugt

$$P_{op} \cdot A = \frac{I_L \cdot \hbar\omega}{\eta_Q \cdot e}$$

Für die NEP setzen wir $I_{sh} = I_L$, sodaß

$$I_L = I_{sh} = \sqrt{2 e \cdot (I_0 + I_L) \cdot \Delta f} =$$

und mit $I_0 \ll I_L$ erhalten wir

$$I_L = 2 e \cdot \Delta f$$

Die optische Leistung erforderlich bei einer Bandbreite Δf ist gibt

$$NEP = P_{op} \cdot A = \frac{2 \cdot \hbar\omega \cdot \Delta f}{\eta_Q}$$

Ist jetzt $I_0 \gg I_L$ bekommen wir

$$I_L \sim \sqrt{2 \cdot e \cdot I_0 \cdot \Delta f}$$

$$NEP = P_{op} \cdot A = \frac{\sqrt{2e \cdot I_0 \cdot \Delta f} \cdot t_W}{\eta_Q \cdot e}$$

Die Nachweisgrenze D (Detektivität) ergibt sich damit zu

$$D = \frac{1}{NEP} = \frac{e}{t_W} \cdot \frac{\eta_Q}{\sqrt{2 \cdot e \cdot I_0 \cdot \Delta f}}$$

Sowohl die Detektivität als auch die NEP hängen von der Fläche als auch der Bandbreite des Detektors ab. Es wird deshalb eine von diesen Parametern unabhängige Größe definiert, nämlich die "spezifischen Detektivität" oder "bezogenen Nachweisgrenze"

$$D^* = \frac{\sqrt{A \cdot \Delta f}}{NEP} = \frac{e}{t_W} \cdot \frac{\eta_Q}{\sqrt{2 e \cdot J_0}}$$

In der Wahl eines Detektors, wählt man nachdem die Bandbreiten erforderlichen erfüllt sind, denjenigen Detektor mit dem höchsten D^* aus.

Folie 209

(Bild aus SBE)

spezifische Detektivität D*

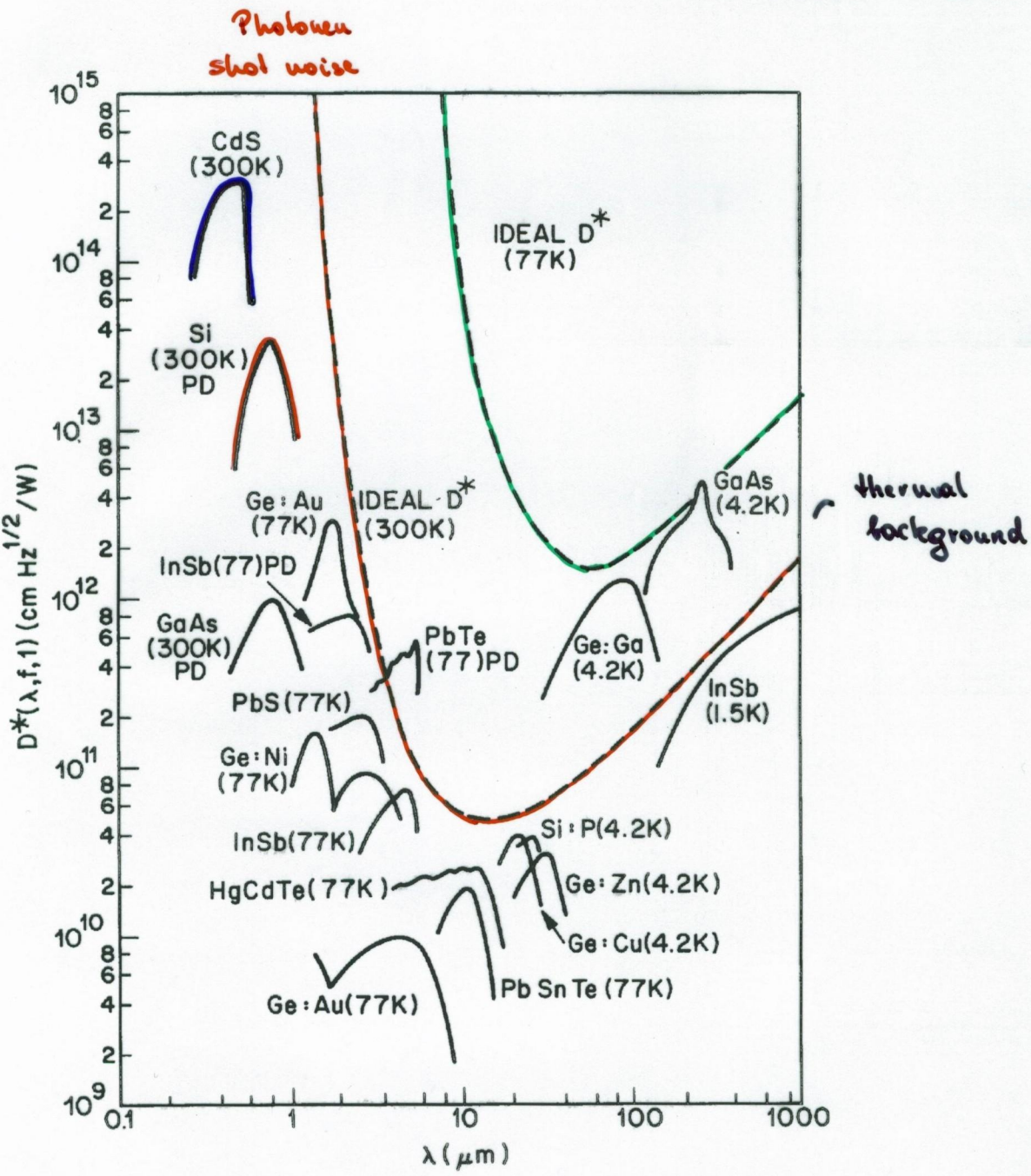

Materialien für optische Detektoren

InGaAs (Tunable E_g)	• Excellent material for long haul communications (at 1.55 μm) • Can be lattice matched to InP
AlGaSb (Tunable E_g)	• Excellent optical properties • Can be used for long haul communications • Suffers from poor substrate availability, since it has to be grown on GaSb, whose technology is not matured
InGaAsP (Tunable E_g)	• Suitable for both 1.55 μm and 1.3 μm applications for long haul applications • Can be lattice matched to InP substrates
HgCdTe (Tunable E_g)	• Excellent material for long wavelength applications in night vision and thermal imaging • Can be used for 1.55 μm and 1.3 μm, but the technology is not as advanced as the InP based technology
Si (E_g = 1.1 eV)	• Indirect material with small α near the bandedge • Has high β_{imp}/α_{imp} ratio and can be used in high performance avalanche photodiodes for local area network (LAN) applications • Not suitable for long haul communication at λ = 1.55 μm or 1.3 μm
Ge (E_g = 0.7 eV)	• Indirect material with small α near the bandedge • Has high β_{imp}/α_{imp} ratio and can be used for avalanche photodiodes for both local area and long distance communications
GaAs (E_g = 1.43 eV)	• Direct gap material • Not suitable for high quality avalanche detectors, since $\alpha_{imp} \simeq \beta_{imp}$ • Not suited for long distance or LAN applications

Table 7.2: Important semiconductor systems for detectors.

Verschiedene Detektoren:

a) Photostrom in einer p-n-Diode (Solarzelle)

b) Photoleitungsdetektor

c) P-I-N Photodetektor

d) Lawinendurchbruchsphotodetektor (APD)

e) Phototransistor

f) Metall - Halbleiter Detektor (MSM)

g) Quantum-Well-Intersubband Detektor

ad a) Photoleitung als Detektor

Bei Einstrahlung von Licht auf einen wenig dotierten HL ändert sich die Löcher u. Elektronenkonzentration entsprechend

$$\delta_p = \delta_n = G_L \cdot \tau_p$$

und damit auch die Leitfähigkeit

$$\Delta\sigma = e \cdot \delta_p \cdot (\mu_n + \mu_p)$$

$$\sigma = e \cdot (\mu_n \cdot n_0 + \mu_p \cdot p_0)$$

$$\sigma + \Delta\sigma = e\,(\mu_n \cdot (n_0 + \delta_n) + \mu_p \cdot (p_0 + \delta_p))$$

$$= \sigma + e \cdot (\mu_n \cdot \delta_n + \mu_p \cdot \delta_p)$$

$$= \sigma + e \cdot \delta_p \cdot (\mu_n + \mu_p) \qquad (\delta_n = \delta_p)$$

$$\Delta\sigma = e \cdot \delta_p \cdot (\mu_n + \mu_p)$$

$$J = J_{dark} + J_L = (\sigma_0 + \Delta\sigma) \cdot \vec{F}$$

$$I_L = J_L \cdot A = e \cdot \delta_p \cdot (\mu_n + \mu_p) \cdot F \cdot A$$

$$\boxed{I_L = e \cdot G_L \cdot \tau_p \cdot (\mu_n + \mu_p) \cdot A \cdot F}$$

Zur Erinnerung: $\mu_n \cdot F = v_e$ $\mu_u \cdot F = v_u$ .. Geschwindigkeit

Bei hohen elektrischen Feldern gilt, daß

$\mu_n \cdot F$ und $\mu_p \cdot F$ einfach die Sättigungsgeschwindigkeiten sind

die unabhängig von der Feldstärke sind.

Definition der Transitzeit t_{tr}

$$t_{tr} = \frac{L}{\mu_n \cdot F}$$

Der Photostrom wird deshalb ausgedrückt durch $\mu_n F$ in termen von t_{tr} und L

$$I_L = e \cdot G_L \cdot \left(\frac{\tau_p}{t_{tr}}\right) \cdot \left(1 + \frac{\mu_p}{\mu_n}\right) \cdot A \cdot L$$

Dies ist der im Stromkreis erzeugte Photostrom

mit

$$I_{Lp} = e \cdot G \cdot A \cdot L$$

Dies wäre der Photostrom, wenn jedes e-h Paar einfach eine Ladung zum Kontakt bringt.

Die Verstärkung des Photoleitungsdetektors ist deshalb

$$G_{ph} = \frac{I_L}{I_{Lp}} = \frac{\tau_p}{t_{tr}} \cdot \left(1 + \frac{\mu_p}{\mu_n}\right)$$

τ_p .. effektive Rekombinationszeit der Überschußladungsträger

Verstärkung erfolgt, da das e^- mehrmals durch das Bauelement geht bevor es rekombiniert

Ist τ_p groß und t_{tr} klein $\neq 0$ hohe Verstärkung

in Si gain bis 1000

Bandbreite gain product konstant bei τ_p = konst

nicht so schnell!

Photoleitungsdetektor

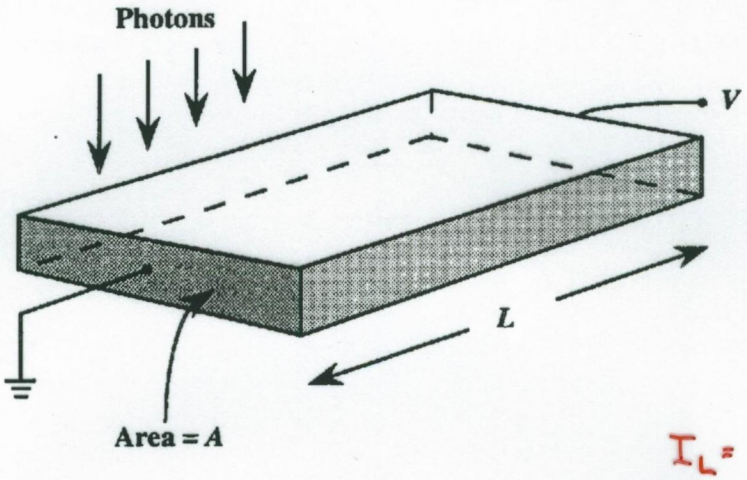

(a)

$\delta p = \delta n = G_L \cdot \tau_p$

$\Delta\sigma = e \cdot \delta p (\mu_n + \mu_p)$

$J = (J_d + J_L) =$

$= (\sigma_0 + \Delta\sigma) \cdot F$

$I_L = J_L \cdot A = e \cdot \delta p (\mu_n + \mu_p) \cdot F \cdot A$

$I_L = e \cdot G_L \cdot \tau_p \cdot (\mu_n + \mu_p) \cdot A \cdot F$

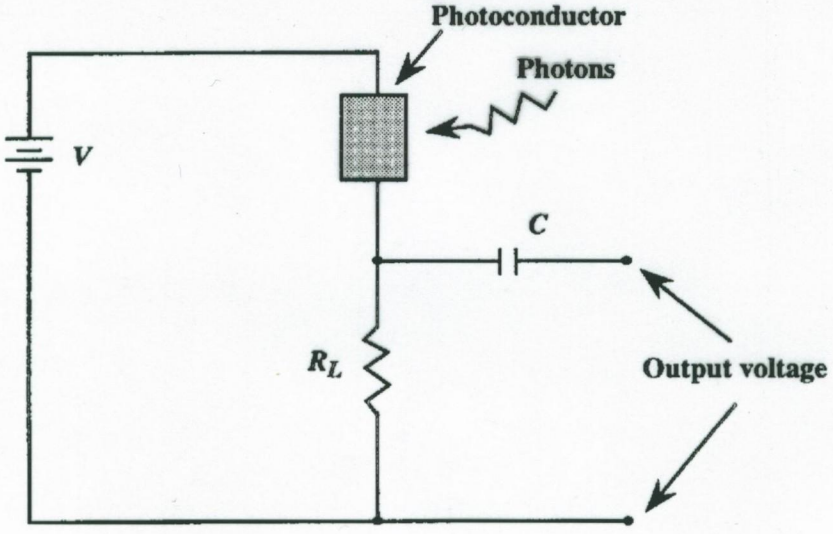

(b)

Figure 7.12: (a) Geometry of a photoconductor of length L and area A. (b) A typical bias circuit for a photodetector. Light causes a change in the resistance of the photoconductor. A blocking capacitor may be used if only the ac signal is to be detected.

P-N Diode

Einfallendes Licht welches in der Verarmungszone W eines p-n Überganges $e^- - h^+$ Paare erzeugt. Diese werden durch das herrschende elektr. Feld getrennt und tragen zum Strom bei

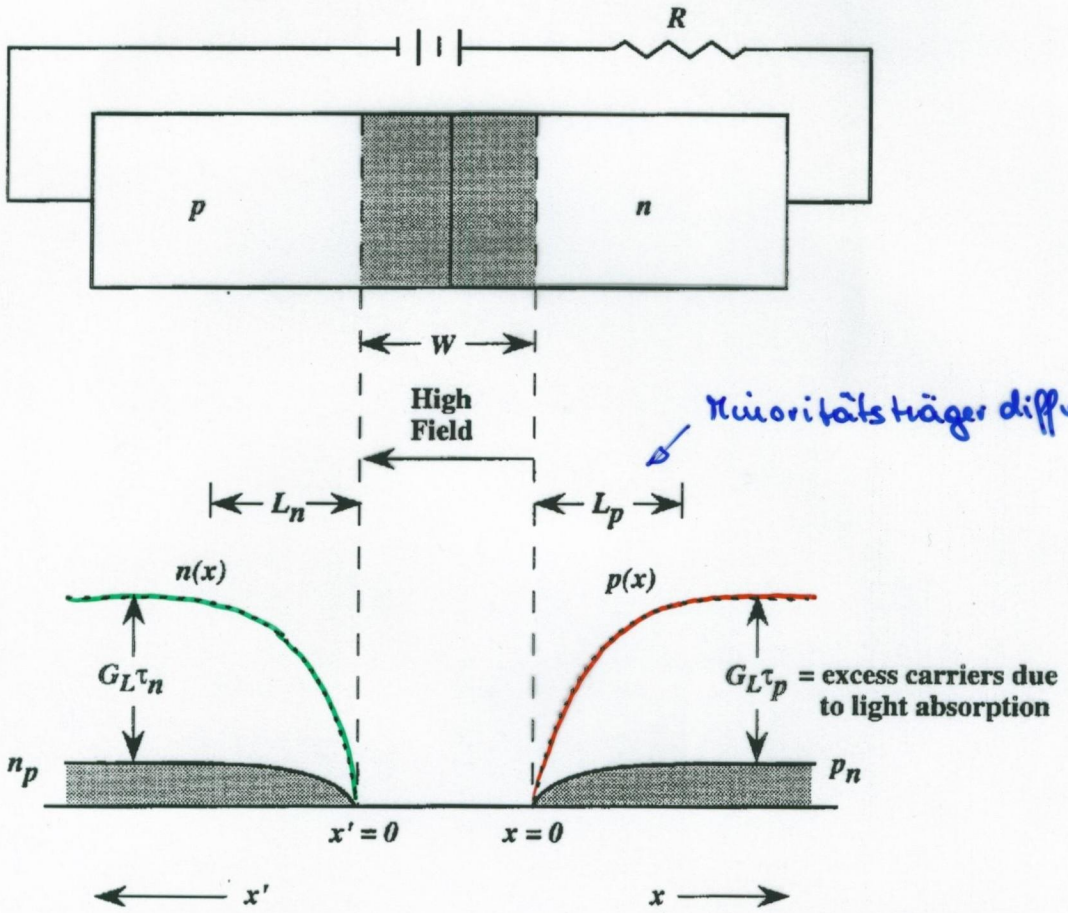

Figure 7.7: A schematic of a p-n diode and the minority carrier concentration in absence and presence of light. The minority charge goes to zero at the depletion region edge due to the high field which sweeps the charge away. The equilibrium minority charge is p_n and n_p in the n- and p-sides, respectively.

$G_L(x) = \text{konst}$

$$I_L = A \cdot e \cdot \int_0^{x'} G_L(x)\,dx = A \cdot e \cdot G_L \cdot W$$

$$I_{pL} = A \cdot e \cdot D_p \cdot \frac{d\,\delta p}{dx}\Big|_{x=0} = e \cdot G_L \cdot L_p \cdot A$$

$$I_{nL} = A \cdot e \cdot D_n \cdot \frac{d\,\delta n}{dx}\Big|_{x'=0} = e \cdot G_L \cdot L_n \cdot A$$

$$I_L = I_{nL} + I_{pL} + I_L = e \cdot G_L \cdot (L_p + L_n + W) \cdot A$$

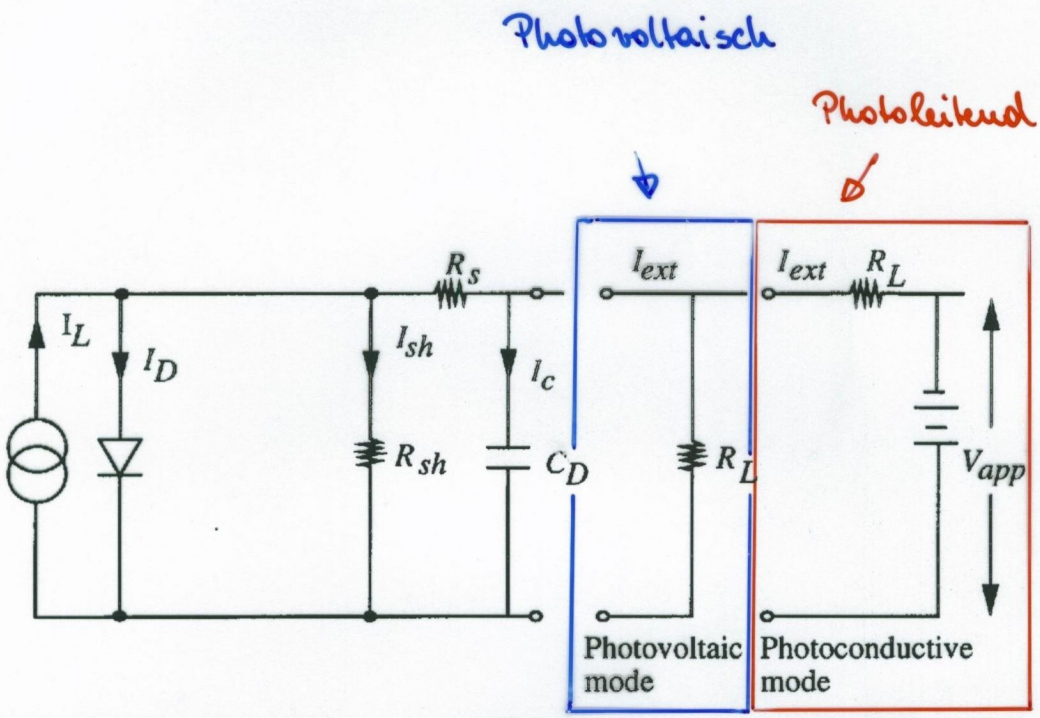

Figure 7.8: The equivalent circuit of a photodiode. The device can be represented by a photocurrent source I_L feeding into a diode. The device's internal characteristics are represented by a shunt resistor R_{sh} and a capacitor C_D. R_s is the series resistance of the diode. In the photovoltaic mode (used for solar cells and other devices) the diode is connected to a high resistance R_L, while in the photoconductive mode (used for detectors) the diode is connected to a load R_L and a power supply.

Diodenkennlinie

$$I = I_0 \left[\exp\{\ \} - 1 \right] \Rightarrow |I| \quad \text{weil negativ}$$

bei externer Last:

$$I = I_L + I_0 \left[1 - \exp\left\{ \frac{e(V + R_s I)}{m \cdot k_B T} \right\} \right]$$

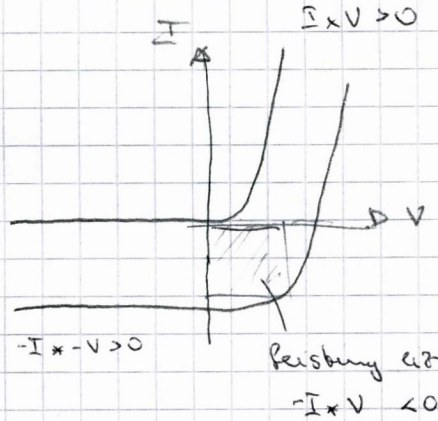

Solarzellen: wichtige Anwendung zur Konversion

a) SZ arbeiten ohne externe Spannungsquellen

$$I = 0 = I_L - I_0 \left[\exp\left(\frac{eV_{oc}}{mkT} \right) - 1 \right]$$

open circuit voltage:

$$\Rightarrow V_{oc} = \frac{m \cdot kT}{e} \cdot \ln\left(1 + \frac{I_L}{I_0} \right)$$

Der zweite Fall ist wenn der Ausgang kurzgeschlossen

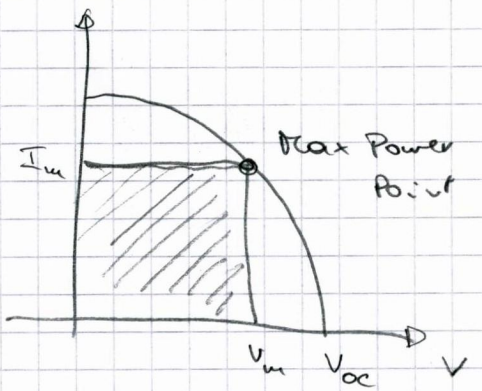

b) kurzgeschlossen

$$I = I_{sc} = I_L$$

Elektrische Leistung: (die maximale Leistung

$$P = I \times V = I_L \cdot V - I_0 \cdot \left[\exp\left(\frac{eV}{kT} \right) - 1 \right]$$

Leistungskonversion:

$$\eta_{conv} = \frac{P_M}{P_{in}} \times 100 \text{ (prozent)} = \frac{I_m \cdot V_m}{P_{in}} \times 100 \text{ prozent}$$

Füllfaktor

$$F_f = \frac{I_m \cdot V_m}{I_{sc} \cdot V_{oc}} \sim 0.7$$

14.1.4 *n-i-p-i* Superlattice Photoconductor [10, 11]

Recently, modulation doping in semiconductors has been introduced for novel device applications. An interesting example is a GaAs doping superlattice used as a photoconductor. For an extensive review of the compositional and doping superlattices, see Refs. 10 and 11. Here we consider a GaAs doped periodically *n*-type and *p*-type separated by intrinsic regions as shown in Fig. 14.3a. The electric field profile $E(z)$ can be obtained by noting that $dE(z)/dz = \rho(z)/\varepsilon$, where $\rho(z) = +qN_D$ in the *n*-doped regions, $-qN_A$ in the *p*-doped regions, and zero in the intrinsic regions. Therefore, $E(z)$ is either a linear profile with a positive slope qN_D/ε in *n* regions, a negative slope $-qN_A/\varepsilon$ in *p* regions, or a zero slope in the intrinsic regions (Fig. 14.3b). The potential profile for the conduction band edge $E_C(z) = -q\varphi(z) = +q\int_{-\infty}^{z} E(z')\,dz'$ is the integral of the electric field profile and is shown in Fig. 14.3c.

For an incident light with energy above the band gap, the photogenerated carriers will fall to the band edge and will drift or diffuse to the valleys of each band, as shown in Fig. 14.3c. The electrons are separated from the holes in real space, resulting in a very long recombination lifetime τ_n. This enhancement of a long lifetime has been found to be many orders of magnitude larger than the bulk carrier lifetime. Since the photocurrent response is proportional to $G_0\tau_n$, an extremely large responsivity using the *n-i-p-i* superlattice as a photoconductor can be designed.

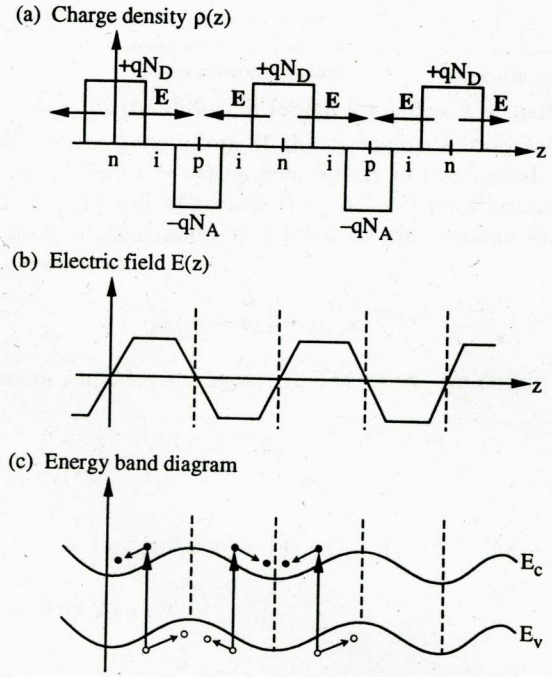

Figure 14.3. (a) The charge density profile due to ionized donors and acceptors in an *n-i-p-i* doping superlattice using the depletion approximation. (b) The electric field profile due to the charge distribution in (a). Notice that the electric field $\mathbf{E} = \hat{z}E(z)$ is alternating between positive and negative directions. (c) The energy band diagram of the *n-i-p-i* superlattice. The photogenerated electron–hole pairs are separated in real space because of the band profiles.

14.2 *p-n* JUNCTION PHOTODIODES [12–15]

Consider a *p-n* junction photodiode as shown in Fig. 14.4a. The charge distribution $\rho(x)$, the electric field $E(x)$ and the potential energy profile under the depletion approximation have been discussed in Chapter 2. Here we investigate the photocurrent response if the diode is illuminated by a uniform light intensity, described by a generation rate $G(x,t)$, which is the number of electron–hole pairs created per unit time per unit volume. Let us focus on the *n* side of the diode.

The charge continuity equation is given by (2.4.2)

$$\frac{\partial p_n}{\partial t} = G(x,t) - \frac{\delta p_n}{\tau_p} - \frac{1}{q}\frac{\partial}{\partial x}J_p(x) \qquad (14.2.1)$$

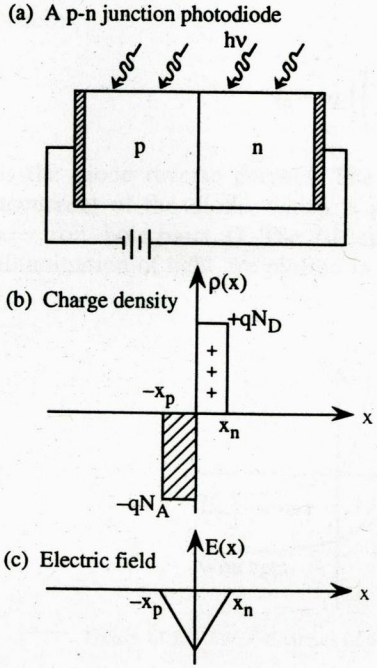

Figure 14.4. (a) A *p-n* junction diode under the illumination of a uniform light. (b) The charge distribution $\rho(x)$ under depletion approximation. (c) The electric field $E(x)$ obtained from Gauss's law.

where $p_n = p_{n0} + \delta p_n$ is the total hole concentration in the n region, p_{n0} is the hole concentration in the absence of any electric or optical injection, and δp_n is the excess hole concentration due to the external injections. The minority (hole) current density in the quasi-neutral region ($x \geq x_n$) is dominated by the diffusion component [12–14], as discussed in Chapter 2:

$$J_p(x) \simeq -qD_p \frac{\partial p_n}{\partial x} \tag{14.2.2}$$

Since p_{n0} is independent of x and t, we have at steady state, if $G(x,t) = G_0$ is independent of x and t,

$$D_p \frac{\partial^2}{\partial x^2} \delta p_n - \frac{\delta p_n}{\tau_p} = -G_0 \tag{14.2.3}$$

The above equation can be solved by summing the homogeneous and particular solutions:

$$\delta p_n(x) = \underbrace{c_1 e^{-(x-x_n)/L_p} + c_2 e^{(x-x_n)/L_p}}_{\text{homogeneous solution}} + \underbrace{G_0 \tau_p}_{\text{particular solution}} \tag{14.2.4}$$

where $L_p = \sqrt{D_p \tau_p}$ is the diffusion length for holes. The particular solution is due to the optical generation. If the n region is very long, we can set $c_2 = 0$; otherwise, $\delta p_n(x \to \infty) \to +\infty$, which is unphysical. We expect as $x \to +\infty$ that $\delta p_n(x)$ will approach $G_0 \tau_p$ = total photogenerated holes. At $x = x_n$, the hole concentration is pinned by the voltage bias V with the exponential dependence

$$p_n(x = x_n) = p_{n0} e^{qV/k_B T} \tag{14.2.5}$$

if the Boltzmann statistics are assumed. Therefore, we obtain

$$\delta p_n(x_n) = p_{n0}(e^{qV/k_B T} - 1) \tag{14.2.6}$$

and

$$\delta p_n(x) = \left[p_{n0}(e^{qV/k_B T} - 1) - G_0 \tau_p \right] e^{-(x-x_n)/L_p} + G_0 \tau_p \tag{14.2.7}$$

The current density $J_p(x)$ is

$$\begin{aligned} J_p(x) &\simeq -qD_p \frac{\partial}{\partial x} \delta p_n(x) \\ &= q \frac{D_p}{L_p} \left[p_{n0}(e^{qV/k_B T} - 1) - G_0 \tau_p \right] e^{-(x-x_n)/L_p} \end{aligned} \tag{14.2.8}$$

We obtain $J_p(x)$ at the boundary of the depletion region x_n as

$$J_p(x_n) = q \frac{D_p}{L_p} p_{n0}(e^{qV/k_B T} - 1) - qG_0 L_p \tag{14.2.9}$$

where the first term is due only to the voltage bias, and the last term is due to optical generation. We see that only that portion of the photogenerated holes within a diffusion length L_p away from the depletion boundary can diffuse (and survive) to the depletion region and be swept across the depletion region by the electric field and collected as the photocurrent by the external circuits. This means that the majority of the carriers on the p side have to supply this current immediately. A parallel (or dual) approach for the electron current density at $x = -x_p$ gives

$$J_n(-x_p) = q \frac{D_n}{L_n} n_{p0}(e^{qV/k_B T} - 1) - qG_0 L_n \tag{14.2.10}$$

The total current I is the sum of $J_p(x_n)$ and $J_n(-x_p)$ multiplied by the cross-sectional area of the diode A:

$$\begin{aligned} I &= A\left[J_p(x_n) + J_n(-x_p) \right] \\ &= I_0(e^{qV/k_B T} - 1) - qAG_0(L_p + L_n) \end{aligned} \tag{14.2.11}$$

where

$$I_0 = qA\left(\frac{D_p}{L_p} p_{n0} + \frac{D_n}{L_n} n_{p0} \right) \tag{14.2.12}$$

is the diode reverse current. The last term, $-qAG_0(L_p + L_n)$, is the photocurrent of the diode, which is proportional to the generation rate of the electron–hole pairs, G. The I-V curves of a photodiode with and without the illumination of light are plotted in Fig. 14.5. When $G_0 = 0$, the diode reverse

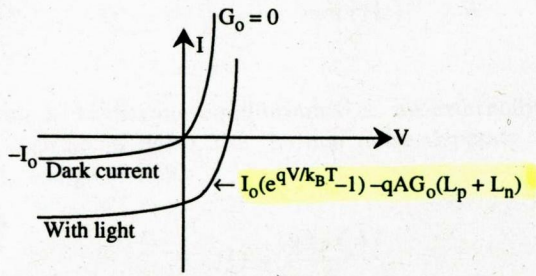

Figure 14.5. The I-V curves of a photodiode with and without illumination.

current $-I_0$ is the dark current, which is usually very small compared with the photocurrent $I_{ph} \simeq -qAG_0(L_p + L_n)$ under a reverse bias condition. Therefore, the photocurrent is proportional to the generation rate G_0, which is proportional to the incident optical power P_{opt}.

The problems with the *p-n* junction photodiodes are as follows:

1. Optical absorption within the diffusion lengths L_p and L_n is very small, that is, over narrow regions of L_p and L_n near the depletion region. Since L_p and L_n are very small, the contributions of the photocurrents are not effective.
2. The diffusion process is slow, which results in a slow photoresponse if the optical intensity varies with time.
3. The junction capacitance C_j is simply $\varepsilon A/x_w$, where x_w is the total depletion width derived in (2.5.24) simplified for a homojunction diode with $\varepsilon_p = \varepsilon_N = \varepsilon$:

$$C_j = A\left[\frac{q\varepsilon}{2(V_0 - V)}\frac{N_D N_A}{N_D + N_A}\right]^{1/2} \tag{14.2.13}$$

which can slow down the response by the RC_j time delay. For example, if $A = (1\text{ mm})^2$, $\varepsilon = 11.7\varepsilon_0$, $N_D = 10^{15}\text{ cm}^{-3} \ll N_A$ for a p^+-n photodiode, and $-V = 10V \gg V_0$, we obtain $C_j \simeq 30$ pF and the 3-dB cutoff frequency $f_{3dB} = 1/(2\pi RC_j) = 100$ MHz for $R = 50\ \Omega$.

R_0A Product [15]. A useful figure of merit for the *p-n* junction photodiodes is the R_0A product. Since the photodiode is operated at zero-bias voltage in many direct detection applications, the differential resistance at zero-bias voltage R_0 multiplied by the junction area A is commonly used:

$$(R_0A)^{-1} = \frac{1}{A}\frac{dI}{dV}\bigg|_{V=0} = \frac{dJ}{dV}\bigg|_{V=0} \tag{14.2.14}$$

So far, we have derived the dark current I_0 contributed by the diffusion processes in this section. Using (14.2.11) and (14.2.12), we obtain

$$\begin{aligned}(R_0A)^{-1} &= \frac{q^2}{k_BT}\left(\frac{D_p}{L_p}p_{n0} + \frac{D_n}{L_n}n_{p0}\right)\\ &= \frac{q^2}{k_BTn_i^2}\left(\frac{D_pN_D}{L_p} + \frac{D_nN_A}{L_n}\right)\\ &= \frac{q}{n_i^2}\sqrt{\frac{q}{k_BT}}\left(N_D\sqrt{\frac{\mu_p}{\tau_p}} + N_A\sqrt{\frac{\mu_n}{\tau_n}}\right)\end{aligned} \tag{14.2.15}$$

where we have used the relations $p_{n0} = N_D/n_i^2$, $n_{p0} = N_A/n_i^2$, and the Einstein relations $D_p/\mu_p = D_n/\mu_n = k_BT/q$. The first term in (14.2.15) is the contribution to $1/(R_0A)$ from the diffusion current on the n side of the photodiode, and the second term is from the diffusion current on the p side. There can also be other contributions to R_0A products, such as the generation–recombination current in the space-charge region, the surface leakage current, and the interband tunneling current, which depend on the material properties, device geometry, and surface conditions.

For a root-mean-square photon flux density Φ (number of photons per second per unit area) of monochromatic radiation at a wavelength λ, we can write the rms photocurrent

$$i_p = q\eta\Phi A = q\eta\frac{P_\lambda}{h\nu} \tag{14.2.16}$$

where A is the photodetector illumination area, $\Phi = P_\lambda/(h\nu A)$, P_λ is the root-mean-square input optical power at λ ($P_\lambda = p_{rms} = mP_{opt}/\sqrt{2}$), and η is the quantum efficiency of the photodiode including the effects of the internal quantum efficiency, the reflection, and the absorption depth. The current responsivity is therefore

$$R_\lambda = \frac{i_p}{P_\lambda} = \eta\frac{q}{h\nu} \tag{14.2.17}$$

The signal-to-noise ratio S/N (current) is

$$\frac{S}{N} = \frac{i_p}{\sqrt{\langle i_n^2\rangle}} = \frac{R_\lambda P_\lambda}{\sqrt{\langle i_n^2\rangle}} \tag{14.2.18}$$

The detectivity for the above S/N is defined as

$$D_\lambda^* = \frac{R_\lambda\sqrt{A\,\Delta f}}{\sqrt{\langle i_n^2\rangle}}\ \text{cm (Hz)}^{1/2}/\text{W} \tag{14.2.19}$$

For a photodiode at thermal equilibrium (i.e., no externally applied voltage and no illumination of light), the thermal noise depends on the zero bias resistance R_0 using (14.1.59):

$$\langle i_n^2\rangle = \frac{4k_BT\,\Delta f}{R_0} \tag{14.2.20}$$

When not in thermal equilibrium, the *I-V* curve is

$$I(V) = I_0\left(e^{(qV/k_BT)} - 1\right) - I_{ph} \tag{14.2.21}$$

$$I_{ph} = q\eta\Phi_B A \tag{14.2.22}$$

where Φ_B is the photon flux density due to the background radiation. The mean-squared shot noise current has contributions from three additive terms [15]: (1) a forward current, which depends on voltage, $I_0 \exp(qV_B/k_BT)$, (2) a reverse diode saturation current, and (3) the background radiation induced photocurrent. Since these shot noise currents fluctuate independently, the total mean-squared shot noise current is

$$\langle i_n^2 \rangle = 2q\left(I_0 e^{qV/k_BT}\,\Delta f + I_0\,\Delta f + I_{ph}\,\Delta f\right) \tag{14.2.23}$$

At an operation voltage $V = 0$, $R_0^{-1} = (dI/dV)_{V=0} = qI_0/k_BT$ and (14.2.23) can be written as

$$\langle i_n^2 \rangle = \left(\frac{4k_BT}{R_0} + 2q^2\eta\Phi_B A\right)\Delta f \tag{14.2.24}$$

The detectivity at zero bias voltage is then obtained from (14.2.19)

$$D_\lambda^* = \left(\frac{q\eta}{h\nu}\right)\frac{1}{\left[(4k_BT/R_0A) + 2q^2\eta\Phi_B\right]^{1/2}} \tag{14.2.25}$$

For a thermally limited case, i.e., when the thermal noise is dominant over the background radiation induced signal and other noises, we have

$$(D_\lambda^*)_T = \frac{q\eta}{h\nu}\sqrt{\frac{R_0A}{4k_BT}} \tag{14.2.26}$$

which relates the R_0A product to the thermally limited detectivity. If the photodiode is background radiation limited, which means that the background radiation-induced photocurrent is dominant, we have

$$(D_\lambda^*)_{BLIP} = \frac{1}{h\nu}\sqrt{\frac{\eta}{2\Phi_B}} \tag{14.2.27}$$

which is the detectivity of the background limited infrared photodetector (BLIP).

14.3 *p-i-n* PHOTODIODES [8]

To enhance the responsivity of the photodiode, an intrinsic region used as the major absorption layer is added (Fig. 14.6a). For a light injected from the p^+ side with an optical power intensity I_{opt} (W/cm^2), the generation rate is

$$G(x) = (1 - R)\eta_i\left(\frac{I_{opt}}{h\nu}\right)\alpha e^{-\alpha x} \tag{14.3.1}$$

The optical power intensity I_{opt} is the incident optical power P_{opt} divided by the area A ($I_{opt} = P_{opt}/A$). Note that the total injected number of electrons

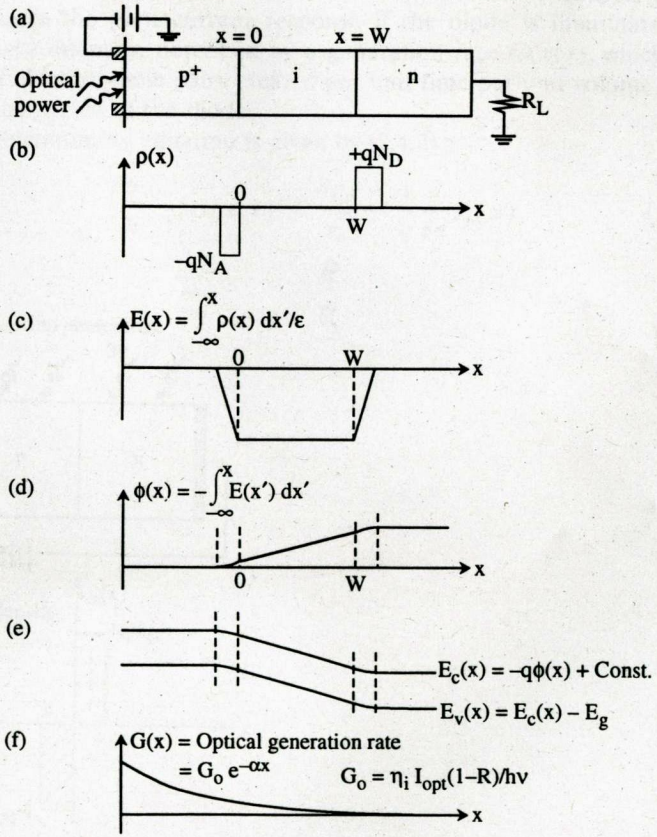

Figure 14.6. (a) A *p-i-n* photodiode under optical illumination from the p^+ side, (b) the charge density $\rho(x)$ under depletion approximation, (c) the static electric field profile $E(x)$, (d) the electrostatic potential $\varphi(x)$, (e) the conduction and valence band edge profiles, and (f) the optical generation rate $G(x)$.

Materialauswahl: für PIN Detektoren

Für Detektoren:

a) hoher Absorptionskoeffizient

- für Übertragungstechnik mit GaAs/GaAlAs ($E_{bg} \sim 1.45$ eV)

  ⇒ Si-Detektoren (Absorptionslänge $W > 10\,\mu m$)

- Langwellenübertragung bei $1.55\,\mu m$

  ⇒ Ge-Detektoren

  für hochgeschwindigkeitsanwendung ist jedoch ein direkter Halbleiter notwendig

  ⇒ InGaAs detektoren

- Nachtsichtgeräte:

  $Hg_x Cd_{1-x} Te$

  InAs

  InSb

  Problem: hoher Dunkelstrom (I_0 der Diode)

  ⇒ Kühlung oft auf LHe_4 oder LN_2

Nach der Auswahl des Materials:

- Minimierung der Oberflächenreflexion (Antireflexbeschichtung)
- Maximierung der Absorption in der Verarmungszone (hohes η)
- Minimierung der Ladungsträgerrekombination (⇒ hochreines Material (keine Störstellen))
- Minimierung der Transitzeit

Für hochfrequenzanwendungen müssen auch RC-konstanten mit berücksichtigt werden wobei $C_D = \frac{\varepsilon \cdot A}{W}$ ← Fläche, ← Transitzeit und R_S ... Serienwiderstand.

⇒ A reduzieren

$W \simeq \frac{1}{\alpha}$ ⇒ $f_{3dB} \simeq \frac{2.4}{2\pi \cdot t_{tr}} \simeq \frac{0.4 \cdot v_{sat}}{W} \simeq 0.4 \cdot \alpha \cdot v_s$

PIN - Dekktor

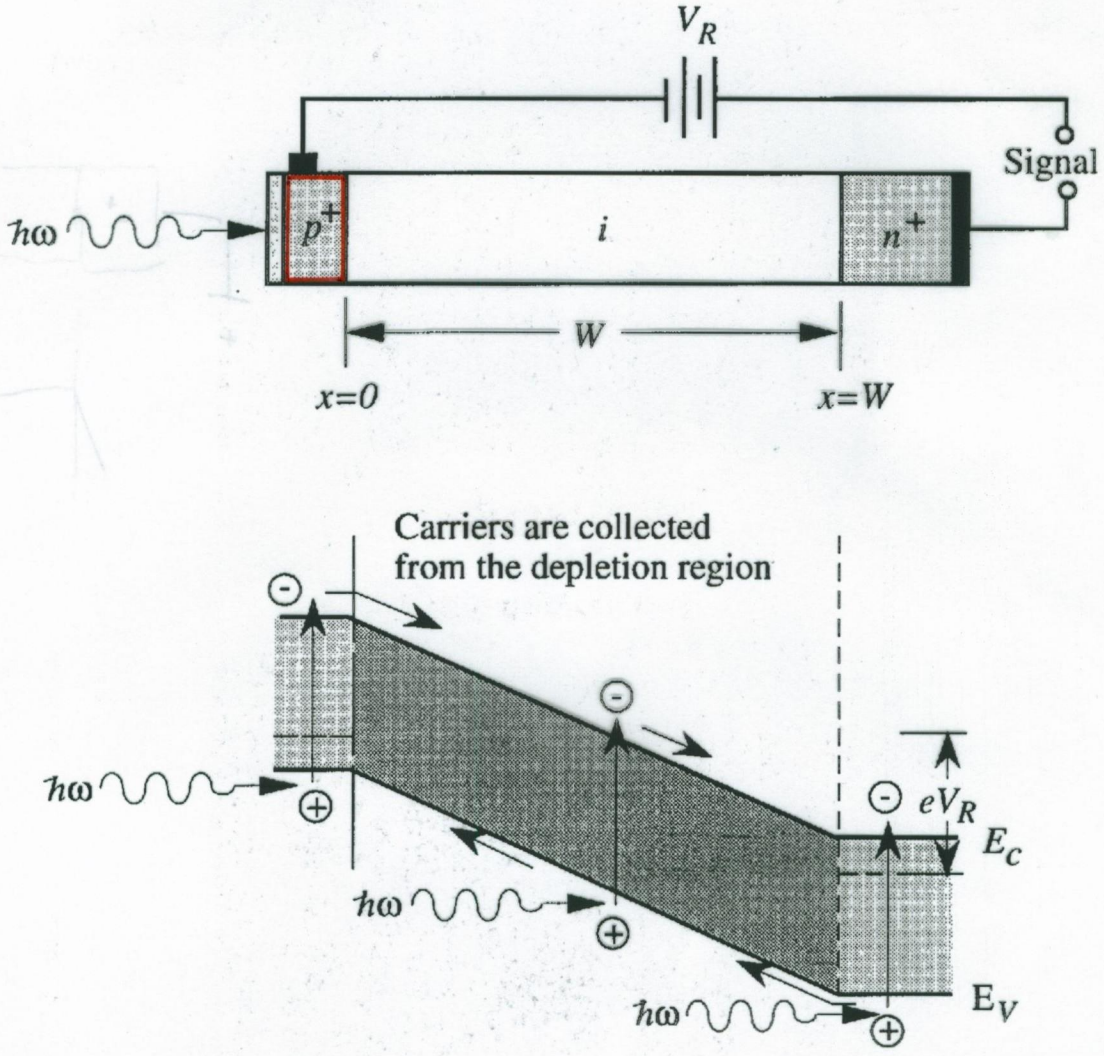

Figure 7.14: A cross-section and energy band profile of a p-i-n detector structure. Carriers generated in the depletion region are collected and contribute to the current. If the intrinsic region is thick, the photocurrent is dominated by carriers collected from the depletion region since the carriers generated in the neutral regions contribute a smaller fraction of photocurrent. Since the photocurrent is dominated by the prompt photocurrent, the device response is fast.

PIN - Detektor

Wird in Sperrrichtung betrieben, jedoch noch nicht so hoch, daß Stoßionisation auftritt.

In Sperrichtung: Dunkelstrom I_0 klein und unabhängig von V

Ladungsträger im i-Bereich (Feld) ⇒ sehr schnell

$$I_L = e \cdot A \int_0^W G_L(x)\,dx$$

$$G_L(x) = \alpha \cdot J_{ph}(0) \cdot \exp(-\alpha x)$$

$$I_L = e \cdot A \cdot J_{ph}(0) \cdot [1 - \exp(-\alpha W)]$$

mit Reflexion: ⇒ Antireflex Beschichtung

$$I_L = e \cdot A \cdot J_{ph}\,(1-R)\,[1 - \exp(-\alpha W)]$$

⇒ Detektor effizienz: (Photostromdichte zum einfallender Fluß)

$$\eta = \frac{I_L}{A \cdot J_{ph}(0)} = (1-R)\,[1 - \exp(-\alpha W)]$$

⇒ kleines R
langes W (transitime) } ⇒ bis 10 GHz ($W \approx 1\,\mu m$)

bei zu großem W wird die Transitzeit zu lang und reduziert deshalb die Schaltgeschwindigkeit des Bauelements

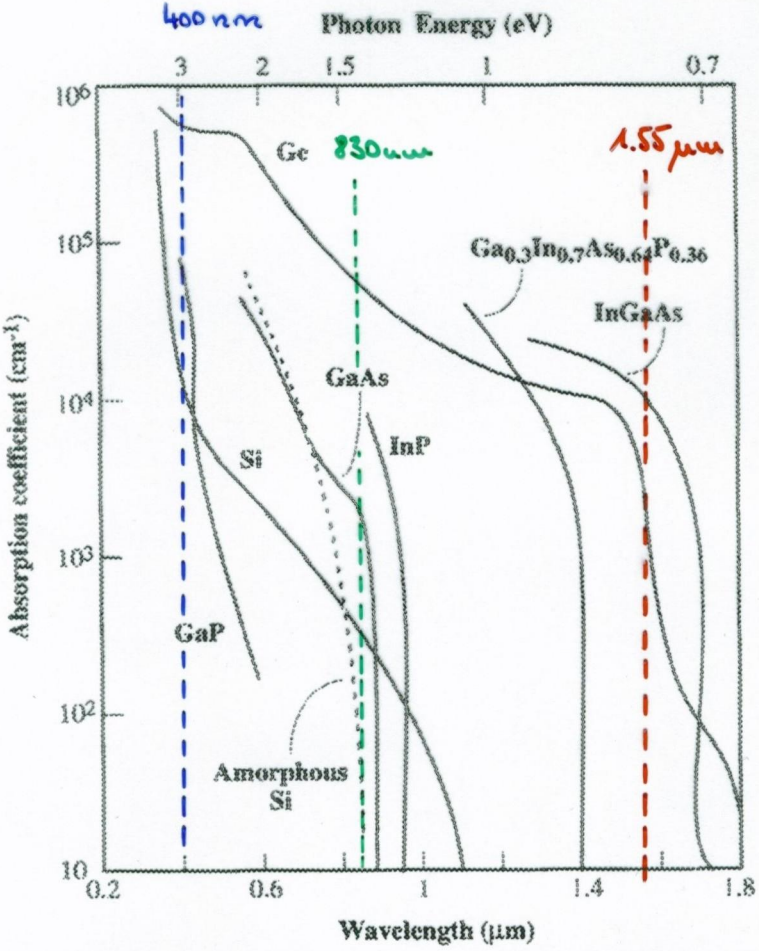

Figure B.4: Absorption coefficient as a function of wavelength for several semiconductors.

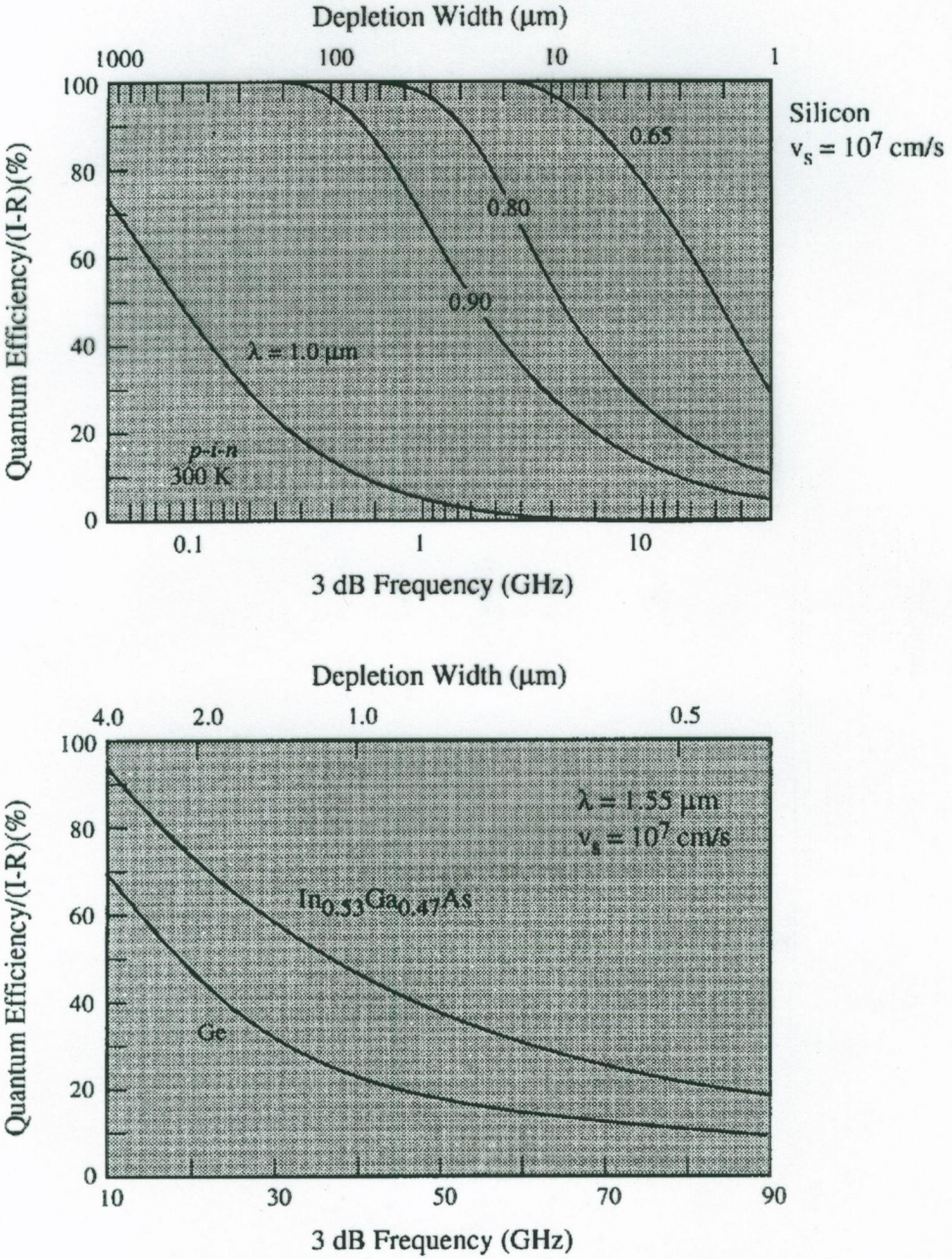

Figure 7.15: a) The 3dB frequency and quantum efficiency tradeoffs in a silicon detector. Results are shown for several wavelengths. b) The high frequency-quantum efficiency tradeoffs in $In_{0.53}Ga_{0.47}As$ and Ge detectors for 1.55 μm radiation.

Der Lawinendurchbruchsdetektor (APD)

Dieser Detektortyp nützt die Stoßionisation oder den Lawinendurchbruch aus um hoch verstärkende Bauelemente zu erhalten.
Während bei der PIN-Diode der Gain höchstens 1 werden kann, können bei der APD sehr hohe Verstärkung erreicht werden.
Beim Lawinendurchbruch erzeugt ein hochenergetisches Elektron ein e-h Paar und vervielfältigt dadurch die von einem Photon erzeugten Ladungsträger. Dieser Prozess erfolgt bei hohen elektrischen Feldern.
Das Ausgangssignal wird deshalb verstärkt.

siehe Folie Fig. 7.16 + B2 + B3

Die Stoßionisationskoeffizienten für Elektronen und Löcher werden α_{imp} und β_{imp} bezeichnet

Wegen der hohen Ladungsträgervervielfältigung werden APD in der optischen Nachrichtenübertragung weit eingesetzt.
Da der Multiplikationsprozess jedoch zufällig ist, ist der Detektor jedoch sehr Rauschbehaftet.
Der Rauschlevel hängt von dem Multiplikationsfaktor und vom

α_{imp}/β_{imp} Verhältnis ab ($\Rightarrow$ Si-Detektoren)

Design Regeln:

- Absorptionsbereich wie bei PIN $\sim \frac{1}{\alpha(\lambda_{vo})}$ $\Rightarrow$ Verarmungszone dickgenug
- Absorptions- und Lawinendurchbruchsbereich sind unterschiedlich im Allgemeinen

  $\Rightarrow$ wichtige Struktur: "reach through" = Durchreichstruktur

  $\Rightarrow$ Fig. 7.17 $\quad u^+ - p - \pi - p^+$

  π... Absorptionsbereich

- Ge-APD leiden unter hohen Dunkelstrom $\Rightarrow$ gain nur $\sim 10-20$

Vor- und Nachteile verschiedener Detektoren

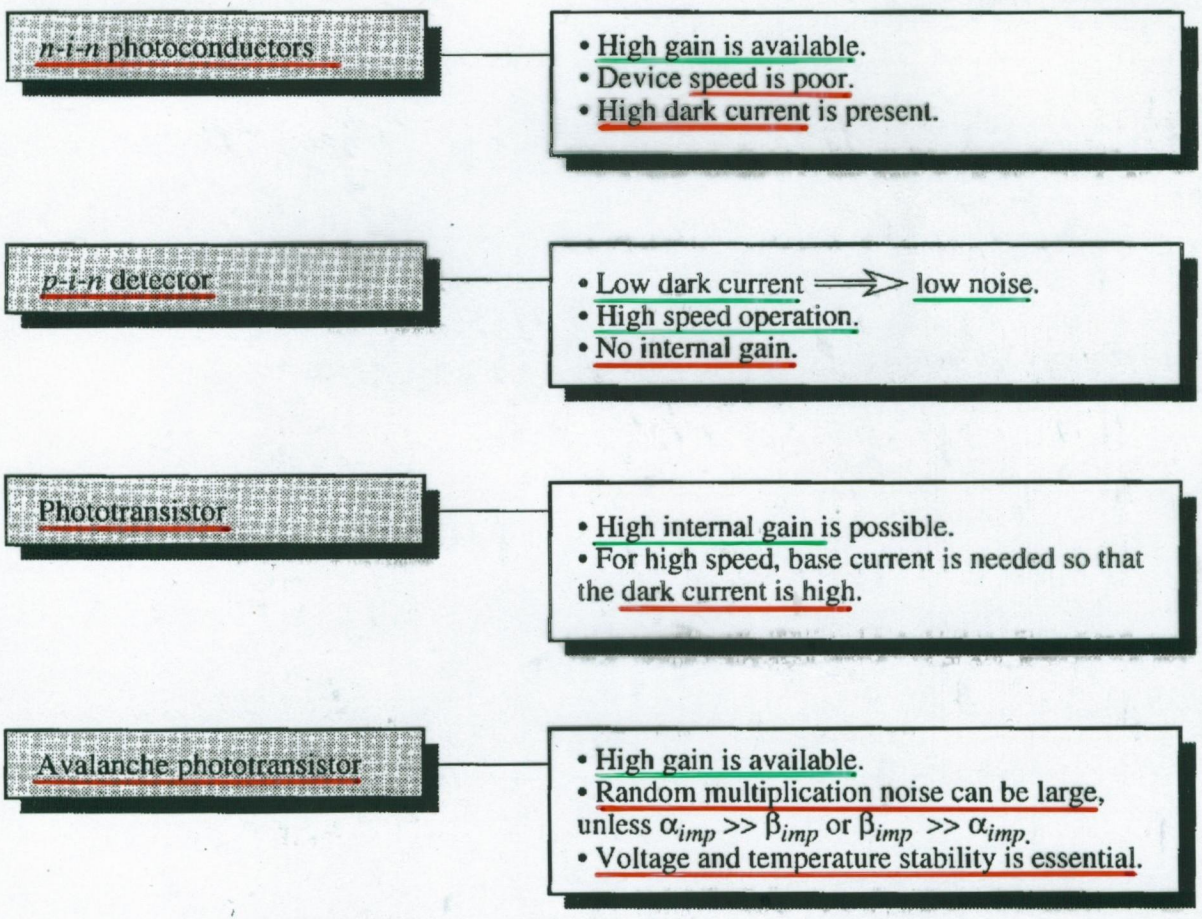

Figure 6.18: A comparison of the advantages and disadvantages of various detectors. The *p-i-n* and APD devices are chosen for high-speed applications. An amplifier is used in the receiver circuit.

TOPICS STUDIED	KEY OBSERVATIONS
Avalanche photodetector, APD	• A reverse biased junction where electric fields are so high as to cause carrier multiplication. • By proper device design, gain of up to 100 can be achieved. • The device is, however, not fast and is quite noisy.
Phototransistor	• A detector based upon bipolar transistor technology. • Current due to carriers generated in the base can be amplified to produce a high gain detector.
Metal-semiconductor detector	• A high performance detector that uses a Schottky barrier to sweep the *e-h* pairs to generate photocurrent. • The device is simple to fabricate and to integrate with other devices.

Table 6.3: Summary table

Verschiedene Dekektoren

TOPICS STUDIED	KEY OBSERVATIONS
Solar cell	• A *p-n* diode operated with no external bias. •Presence of optical intensity creates an output voltage and current which can be used to convert photons to electrical power.
Photoconductive detector	• A simple *n-i-n* (or *p-i-p*) detector in which the conductivity changes when light is incident. •The detector can have high gain if the recombination time is larger than the transit time. This allows an electron to go around the circuit several times before recombining with a hole.
p-i-n detector	• A reverse biased *p-i-n* detector. • The device has high speed, although it has no gain. • Carriers generated in the *i*-region are collected very efficiently to provide a high performance detector.

Table 6.2: Summary table

TOPICS STUDIED	KEY OBSERVATIONS
Shot noise in a detector	Noise produced as a result of the discrete nature of electrons and photons. The random distribution of the particles produce the noise.
Noise Equivalent Power (NEP)	The minimum optical power needed to produce a photocurrent equal to the noise current of the detector.
Detectivity (D,D^*)	Detectivity (D) is defined as the inverse of the NEP. D^* is defined as $D(Af)^{1/2}$ where A is the device area and f is the bandwidth.
Charge coupled devices	An array of MOS and MIS capacitors used to image an optical scene by transferring packets of charges sequentially.

Table 6.4: Summary table

Zusammenfassung - Detektoren

TOPICS STUDIED	KEY OBSERVATIONS
Optical absorption in semiconductors	• Process by which a photon creates *e-h* pairs in semiconductors. • The process can involve an electron moving from a valence band to conduction band *OR* from valence band to an impurity level in the bandgap.

Kenngrößen:

Cutoff wavelength for absorption	In band to band absorption the photon energy must be larger than the bandgap to allow optical absorption.
Responsivity, R	The ratio of the photocurrent to the optical power impinging upon the semiconductor.
Quantum efficiency, η_Q	Tells us what fraction of photons result in *e-h* pairs collected at the contacts.

Table 6.1: Summary table

	Verstärkung "G"	Ansprechzeit/s
Fotoleiter	$1 - 10^6$	$10^{-2} - 10^{-8}$
Sperrschichtfoto-detektoren		
PN- "	1	$10^{-8} - 10^{-10}$
PIN- "	1	$10^{-8} - 10^{-10}$
MS- "	1	10^{-12}
Hetero- "	1	10^{-12}
MIS- "	1	10^{-8}
Lawinenfotodioden	$<10^3$	$10^{-8} - 10^{-10}$
Fototransistor	$<10^3$	$10^{-6} - 10^{-8}$
Fotothyristor	$<10^2$	10^{-6}

Tafel 3.4 Beispiele von Verstärkung und Ansprechzeiten typischer Fotodetektoren

IR - Detektoren

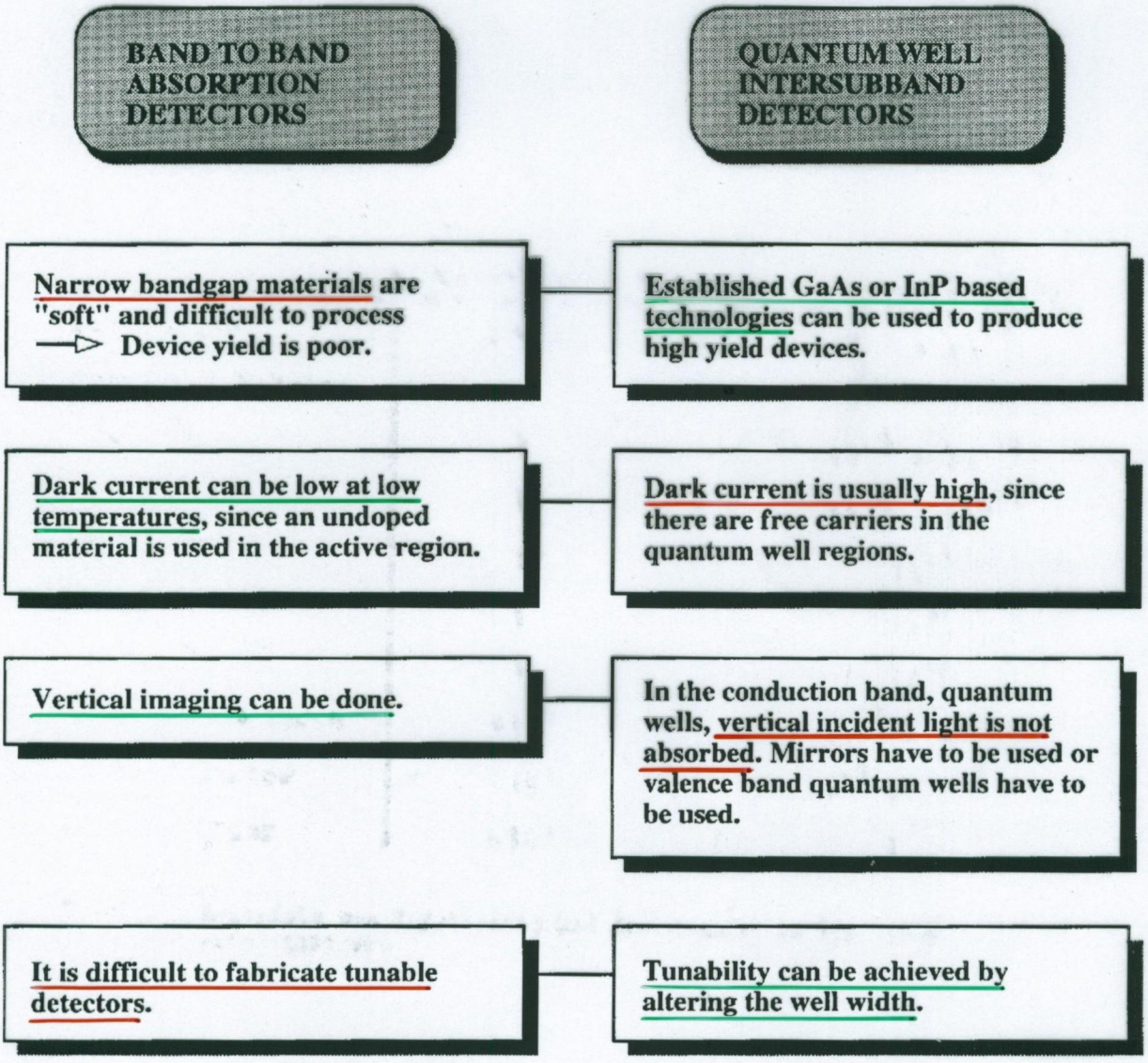

Figure 7.24: A comparison of band to band absorption detectors and quantum well intersubband detectors for long wavelength detectors

7.10 QUANTUM WELL INTERSUBBAND DETECTOR

An important application of detectors is in the area of the detection of long wavelength radiation (λ ranging from 5-20μm). If a direct band to band transition is to be used for such detectors, the bandgap of the materal has to be very small. An important material system in which the bandgap can be tailored from 0 to 1.5 eV is the HgCdTe alloy (see Figs. 7.2 and 7.6). The system is widely used for thermal imaging, night vision applications, etc. However, the small bandgap HgCdTe is a very "soft" material which is very difficult to process. Thus the device yield is rather poor. The quantum well intersubband detector offers the advantages of long wavelength detection using established technologies such as the GaAs technology.

In Fig. 7.23, we show a quantum well which is doped so that the ground state has a certain electron density and the excited state is unoccupied. As discussed in Chapter 4, Section 4.6, when a photon with energy equal to the intersubband separation impinges upon the quantum well, the light is absorbed and the ground state electron is scattered into the excited state.

For the absorption process to produce an electrical signal, one must have the following conditions satisfied:

i) the ground state electrons should not produce a current. If this is not satisfied, there will be a high dark current in the detector. The electrons in the ground state carry current by thermionic emission over the band discontinuity. At low temperatures this process can be suppressed.

ii) It should be possible to extract the excited state electrons from the quantum well so that a signal can be produced. The excited electron state should, therefore, be designed to be near the top of the quantum well barrier, so that the excited electrons can be extracted with ease by an applied electric field.

In Chapter 4, Section 4.6, we had seen that absorption coefficients for the intersubband transitions can approach 10^4 cm^{-1}. Thus a series of multiquantum wells with an effective width of ~ 1.0 μm can be used for efficient detection of light. Also, it is possible to tailor the intersubband separation by either the well width variation or by the barrier height variation. Thus an extremely versatile device can be fabricated.

We had discussed in Chapter 4 that for the conduction band quantum well in which the central cell symmetry of the states is pure s-type, the light is absorbed only if it is incident z-polarized. Here z is the quantum well growth direction. Thus, for vertical incidence, there is no absorption. This is an important drawback for such detectors. One way to overcome this problem is to use etched mirrors on the surface to reflect vertically incident light so that it has a z-polarization. Another way to avoid this is to use the intersubband transitions in the valence band where, due to the mixed nature of the HH and LH states, the z-polarization rule is not valid. However, the poor hole transport properties and the difficulty in reducing the dark current reduce the detector performance. In Fig. 7.24, we show a comparison of the band to band and intersubband

detectors for long wavelength detection

Quantum Well Intersubband Detektor

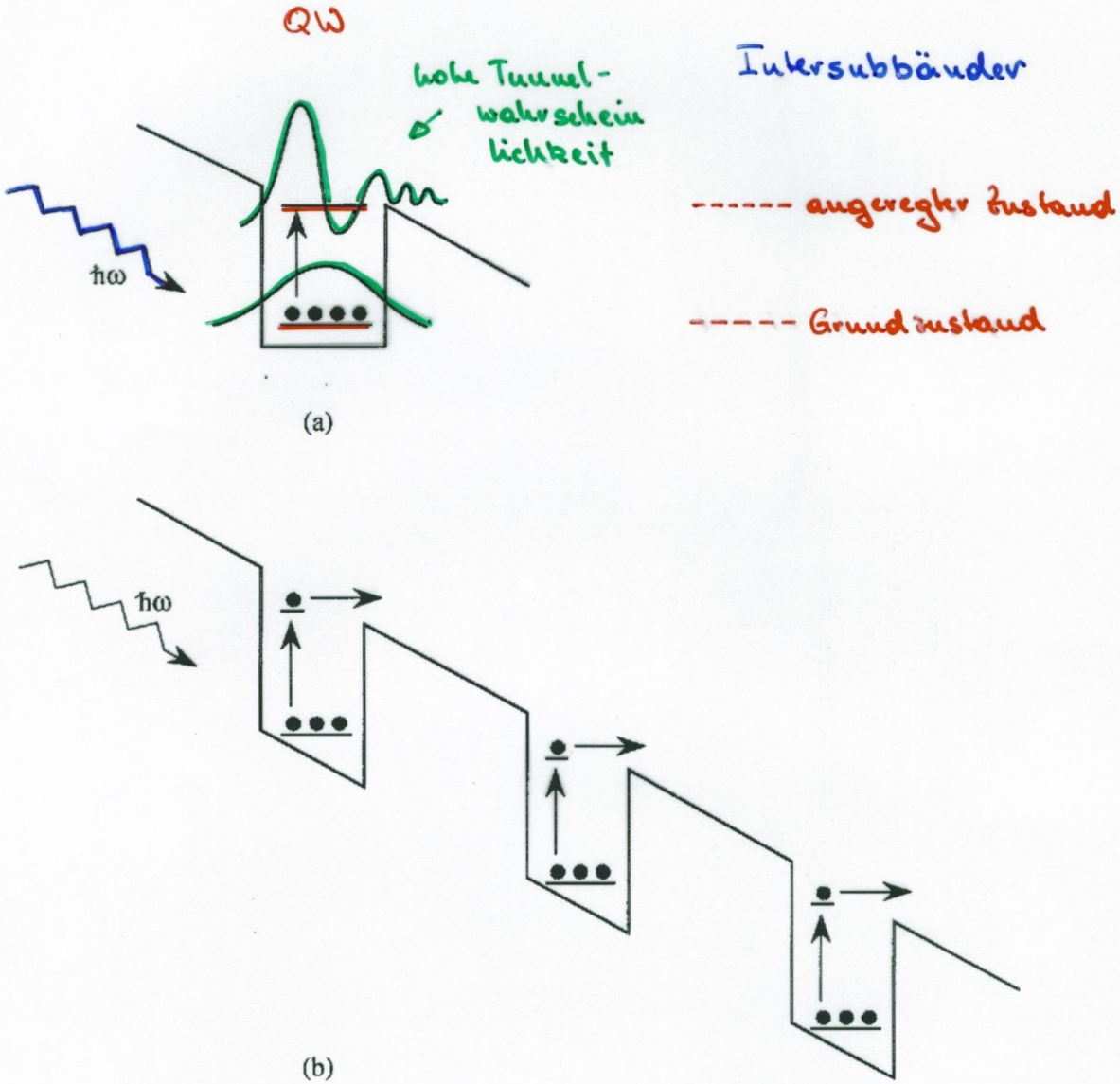

Figure 7.23: (a) A schematic of the electron wavefunction in the ground state and the excited state. The photon causes transitions to the excited state from where the electrons are collected as shown in (b).

7.9 METAL-SEMICONDUCTOR DETECTORS

⟶ An extremely important class of photodetectors involves the use of a Schottky barrier produced between a metal and a lightly doped semiconductor. We have discussed the workings of the Schottky barrier in Chapter 6. As discussed in that chapter, we had seen that a key advantage of the Schottky barrier device is that being a majority carrier device, it does not suffer from speed delays arising from minority carrier lifetime issues.

Mesa a)

Schottky barrier based devices involve two kinds of configuration. In Fig. 7.21a we show a device which is a simple mesa structure with an n^+ layer on a semi-insulating substrate. The active absorbing layer is lightly doped ($N_d \sim 10^{15}$ cm^{-3}) and a thin semitransparent metal layer is deposited on it. The metal film is thick enough to allow the Schottky barrier formation (~300-400 Å) but thin enough to allow light to pass through. For high performance the metal film is coated with dielectric anti-reflection coatings and the device area is kept as small as 10^{-5} cm^2 (~50 μm diameter mesa diodes).

The band profile of the Schottky barrier diode is shown in Fig. 7.21b along. Also shown are the Schottky barrier height $e\phi_{bn}$ and the potential drop across the barrier. When light impinges upon the diode, the diode can respond in two important regimes:

i) $\hbar\omega > e\phi_{bn}$: In this case, electrons can be excited in the metal barrier to overcome the Schottky barrier height. As a result, a photocurrent will flow in the device. This current will add to the dark current in the reverse bias diode.

ii) $\hbar\omega > E_g$: In this case, e-h pairs will be created in the semiconductor. As in the case of the photodiode, the carriers generated in the depletion region will be swept out to produce photocurrent.

In high speed devices the depletion region is less than a micron so that device speeds can be extremely high. With proper design Schottky barrier diodes can operate up to 150 GHz. !

b) MSM

A second class of metal semiconductor detectors is the metal-semiconductor-metal (MSM) detector in which two Schottky barriers are placed in a planar geometry close to each other. In actual design the approach used is the interdigitated scheme shown in Fig. 7.22a. The spacing between the fingers is ~1-5 μm so that when a bias is applied between the contacts, the region between the fingers can be completely depleted.

As seen in Fig. 7.22b, when a bias is applied across the fingers, one junction becomes reverse biased, while the other one becomes forward biased. However, since the semiconductor is depleted, the current in the forward biased junction is not the usual high electron forward bias current. Instead, the dark current in the forward biased junction is due to the hole current injected from the metal over the barrier $e\phi_{bp}$ as shown in Fig. 7.22b. As a result, under a strong applied bias, the dark current of the device is equal to the reverse saturation currents from electrons and holes. As discussed in Chapter 6, we have for the dark current density

$$J = A_n^* T^2 e^{-e\phi_{bn}/k_B T} + A_p^* T^2 e^{-\phi_{bp}/k_B T}$$

where A_n^* and A_p^* are the electron and hole effective Richardson constants. The dark current density is usually higher than that achievable in p-i-n diodes for reasons discussed in Chapter 6. However, sufficiently low dark current can be achieved for most applications.

The MSM detectors are found to have internal gain, often at even low applied biases where impact ionization cannot occur. This suggests the possibility of photoconductive gain enhanced by traps which may capture and re-emit either electrons or holes. MSM diodes have been fabricated in both GaAs and InGaAs systems. Thus these devices can be applicable in both local area networks and long haul communication systems. It is also important to point out that MSM detectors are very attractive for OEIC applications.

$$A_n^* = \frac{m^* \cdot e \cdot k_B^2}{2\pi^2 \cdot \hbar^3} \simeq 120 \left(\frac{m^*}{m_0}\right) \left[A\,cm^{-2}K^{-2}\right] \ldots \text{ eff. Richardsonkonstante}$$

MSM - Detektor

(besonders wichtig, verwendet 2 Schottky barrieren)

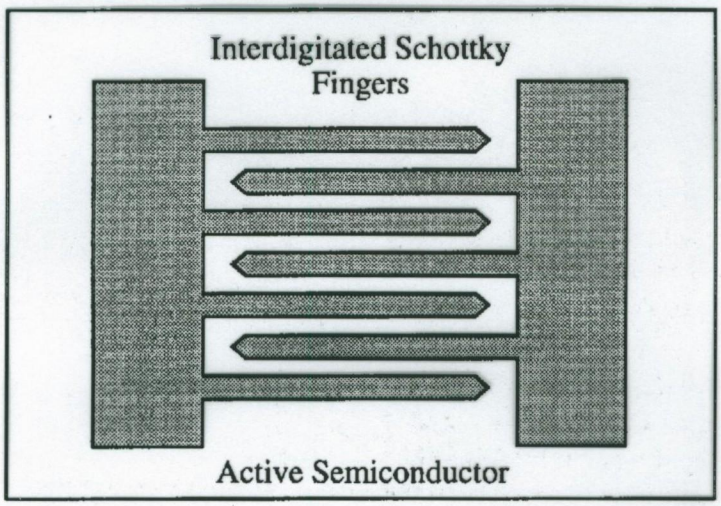

(a)

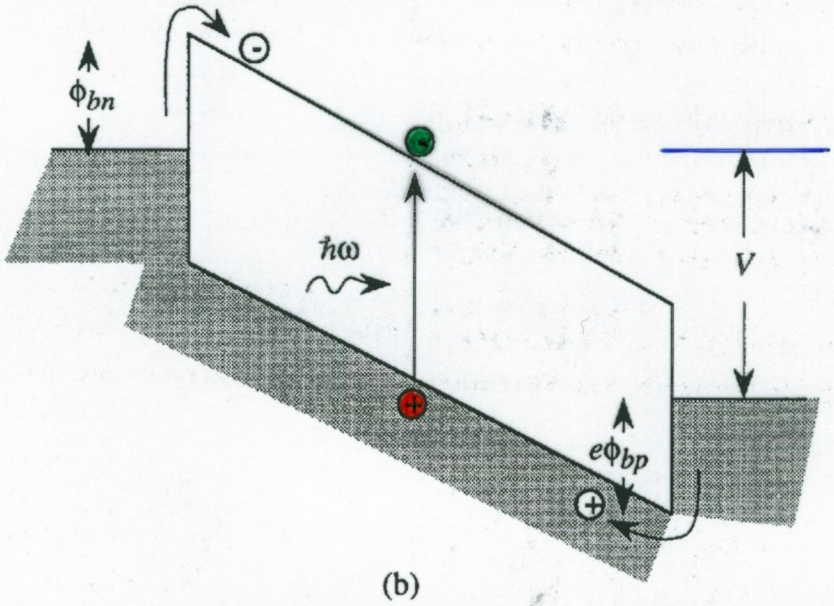

(b)

Figure 7.22: (a) A schematic of the MSM detector using interdigitated Schottky fingers. (b) Band profile of the MSM photodiode under an applied bias.

$$J = A_n^* \cdot T^2 \cdot \exp\left(-\frac{e\phi_{bn}}{k_B T}\right) + A_p^* \cdot T^2 \cdot \exp\left(-\frac{e \cdot \phi_{bp}}{k_B T}\right)$$

$$A_n^* = \frac{m^* \cdot e \cdot k_B^2}{2\pi^2 \cdot \hbar^3} \simeq 120 \left(\frac{m^*}{m_0}\right) \left[A\,cm^{-2}K^{-2}\right] \quad \ldots \text{ eff. Richardsonkonst.}$$

Schottky - Barrieren - Detektor

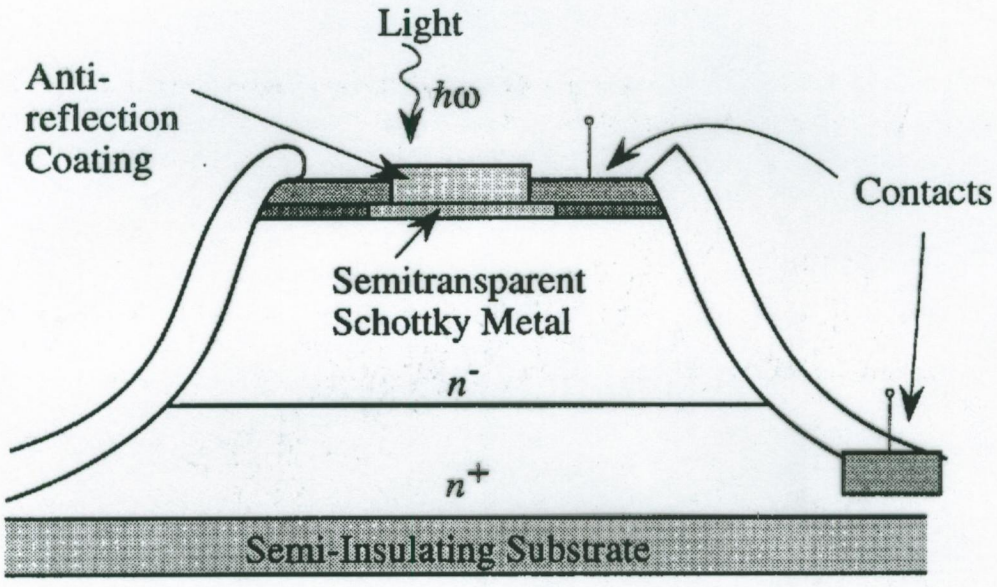

(a)

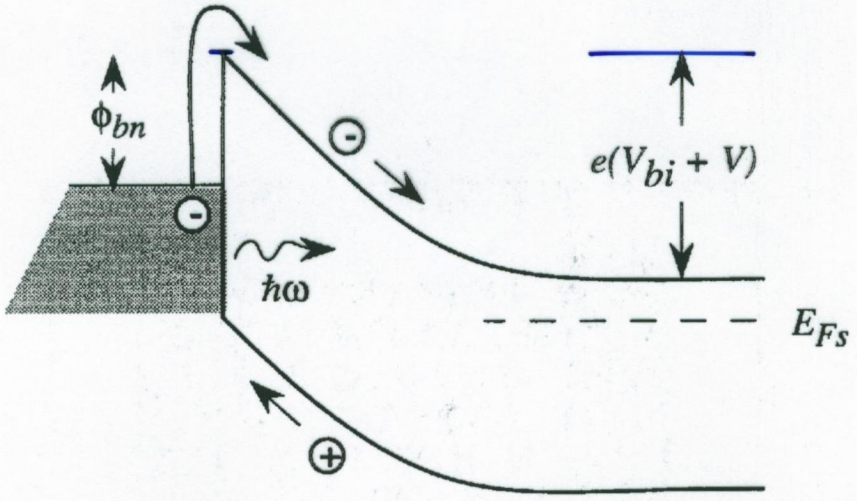

(b)

Figure 7.21: (a) A schematic of the Schottky barrier detector. (b) The band profile of the detector. V_{bi} is the built-in voltage and V is the applied bias.

7.8 THE PHOTOTRANSISTOR

⟶ While the APD discussed above provides very high gain detection, it is an inherently high noise device due to the random nature of the carrier multiplication process. Another device which can produce gain and function as a detector is the bipolar transistor. The phototransistor, the name for the bipolar device used for optical detection, provides high gain due to the transistor action. The device is also a low noise device when compared to an APD.

The bipolar transistor is essentially a device with two coupled p-n diodes, as shown in Fig. 7.20a. The n-p-n transistor is discussed in Appendix D, where we present the underlying operation principles of current gain and transistor action. In this subsection, we will use the results derived in Appendix D to understand how the phototransistor works.

When a bipolar device is biased in the forward active mode (i.e., the emitter-base junction (EBJ) is forward biased and the base-collector junction (BCJ) is reverse biased), the band profile has the form shown in Fig. 7.20b. Normally, in a bipolar transistor, the injection of a small base current causes a small change in the forward bias across the EBJ, causing a large injection of current in the forward biased junction. If the base width is small and the base is of high quality, essentially all of this current is collected in the collector. The current gain, defined as the ratio of the collector and base current, can be quite high (see Example 7.10).

In the case of the phototransistor, the base current is not provided by an external supply (often there is no base contact on the phototransistor), but via an optical signal. Light shining on the device creates electron-hole pairs. These pairs are generated throughout the device, although in an HBT, the emitter can be made of a layer bandgap material and hence, designed to be transparent.

The phototransistor doping levels are designed so that the EBJ depletion width is quite small, while the BCJ depletion width is large, so that the optical signal is absorbed primarily in the BCJ depletion region. This also requires a small width for the base. The photogenerated holes in the BCJ depletion region provide the base current, as shown in Fig. 7.20b. The fraction of the photon current absorbed in the BCJ depletion region is

$$\frac{I_{ph}(BCJ)}{I_{ph}(0)} = \eta\, exp\,(-\alpha W_{bu})[1 - exp\,(-\alpha W_{BCJ})] \tag{7.72}$$

where η is the quantum efficiency of the material ($\eta \sim 1$ for a high quality material);

W_{bu} W_{BC}

the second term is the loss suffered by absorption in the neutral base; and the third term (in the brackets) is the absorption in the depletion region of width W_{BCJ}.

If the phototransistor is designed so that W_{bn} is so small that $exp\,(-\alpha W_{bn}) \sim 1$ and the value of W_{BCJ} is large,

$$I_{ph}(BCJ) \approx \eta I_{ph}(0) \tag{7.73}$$

In this case, essentially all of the optical signal provides a base current, since the high field in the BCJ depletion region injects the holes generated in that region into the base. The optical gain of the device is then ($I_B = eI_{ph}(BCJ)$)

$$\Gamma_G = \frac{I_e}{eI_{ph}(0)} = \frac{\eta I_e}{I_B} = \eta\beta \tag{7.74}$$

where β is the current gain of the device. The dependence of β on the device parameters is discussed in Appendix D (see also Example 7.10).

The phototransistor does not have a very good high frequency response due to the very large capacitance associated with the base-collector junction. However, it finds important uses due to its low noise and high gain.

Phototransistors can be designed using heterojunction bipolar transistors. As discussed in Appendix D, heterojunctions allow one to achieve very high emitter efficiencies and yet achieve low base resistance. Thus, both gain speed and device speed are improved.

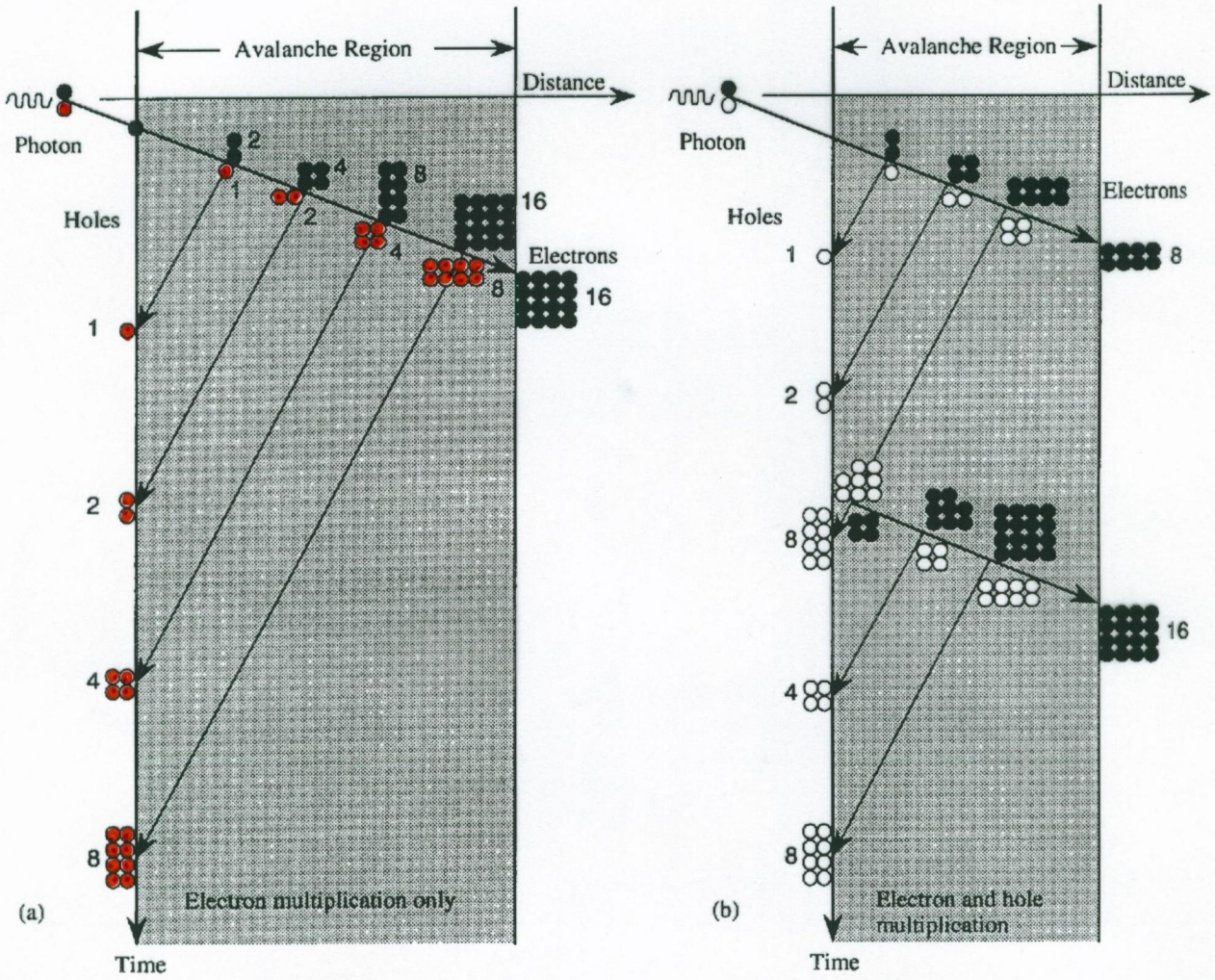

Figure 7.19: The avalanche build-up process shown as a function of time. (a) Only electrons are causing the carrier multiplication. (b) Both electrons and holes are causing the multiplication. (After J. Gowar, *Optical Communication Systems*, Prentice-Hall, Englewood Cliffs, New Jersey (1989).)

The overall device response time is then (defining $\beta_{imp}/\alpha_{imp} = k$)

$$\tau \cong \frac{W_{abs} + M k\, W_{aval}}{v_s(e)} + \frac{W_{abs} + W_{aval}}{v_s(h)} \tag{7.71}$$

It is important to note that for large multiplication values, the produce $\frac{M}{\tau}$ is a constant. The gain-bandwidth product thus remains a constant for a device with large multiplication. This outcome is similar to that observed in the case of photoconductors as well. Thus, if one wants a very high detectivity for very weak optical signals, one has to sacrifice the device speed. Another important conclusion from the Eqn. 7.71 is that gain-bandwidth product can be optimized by choosing a material system with $\alpha_{imp} \gg \beta_{imp}$.

EXAMPLE 7.9 Consider a typical avalanche photodiode with the following parameters:

Incident optical power,	$P_{op} \cdot A$	=	$50\ mW$
Efficiency,	η_{det}	=	90%
Optical frequency,	ν	=	$4.5 \times 10^{14}\ Hz$
Breakdown voltage,	V_B	=	$35\ V$
Diode voltage,	V	=	$34\ V$
Dark current,	I_0	=	$10\ nA$
Parameter n' for the multiplication		=	2

Assume that the series resistance is negligible. Calculate the a) multiplication factor; b) photon flux; c) photocurrent.

a) The multiplication factor from Eqn. 7.67 is

$$M = \left[1 - \left(\frac{34}{35}\right)^2\right]^{-1} = 16.67$$

b) The photon flux is

$$\begin{aligned} I_{ph} &= \frac{P_{op}A}{h\nu} = \frac{(50 \times 10^{-3}\ W)}{(6.625 \times 10^{-34}\ Js)(4.5 \times 10^{14}\ Hz)} \\ &= 1.68 \times 10^{17}\ s^{-1} \end{aligned}$$

c) The unmultiplied photocurrent is

$$\begin{aligned} I_L &= e\eta_{det} I_{ph} = (1.6 \times 10^{-19}\ C)(1.51 \times 10^{17}\ s^{-1}) \\ &= 24.16\ mA \end{aligned}$$

The multiplied photocurrent is

$$M \cdot I_L = (24.16\ mA)(16.67) = 0.4\ A$$

Ladungsträgervervielfältigung

Die APD nützt die Ladungsträgervervielfältigung von Elektronen u. Löchern in hohen elektrischen Feldern aus. Bei solch hohen elektrischen Feldern bewegen sich die Ladungsträger mit der Sättigungsgeschwindigkeit und die Stoß

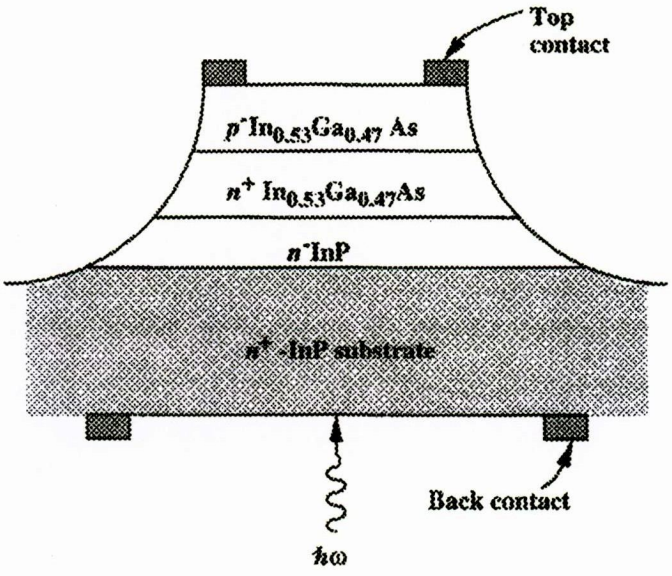

Figure 7.18: A schematic cross-section of a back illuminated InGaAs/InP avalanche photodiode. Due to the short absorption region, in the direct gap semiconductors, one can have the same region for absorption and avalanche processes.

the carriers are moving with saturation velocity and the current is simply proportional to the number of electrons and holes. The electron current has a spatial increment given by

$$\delta i_e = i_e \alpha_{imp} dx + i_h \beta_{imp} dx \tag{7.53}$$

where the first term is the contribution to excess electrons due to the electron current over a distance dx and the second term is due to the excess electrons due to the hole current. We thus have

$$\frac{di_e}{dx} = i_e \alpha_{imp} + i_h \beta_{imp} \tag{7.54}$$

A similar equation exists for the hole current derivative. Even though both the electron and hole current change with spatial position, the total current is constant over the device

$$I = i_e(x) + i_h(x) = \text{constant} \tag{7.55}$$

Let us consider a case where we have an avalanche region extending from $x = 0$ to $x = W$ and at $x = W$, only electrons are injected. Thus we have

$$i_h(W) = 0; \qquad i_e(W) = I \tag{7.56}$$

Expressing $i_h(x)$ in terms of $i_e(x)$ and I by using Eqn. 7.55, we get from Eqn. 7.54

$$\frac{di_e(x)}{dx} - (\alpha_{imp} - \beta_{imp}) i_e(x) = \beta_{imp} I \tag{7.57}$$

This equation is of the form

$$\frac{dy}{dx} + Py = Q \tag{7.58}$$

and has a standard solution given by

$$i_e(x) = \frac{i_e(0) + \int_0^x \beta_{imp} I \; exp\left\{-\int_0^x (\alpha_{imp} - \beta_{imp})dx'\right\} dx}{exp\left\{-\int_0^x (\alpha_{imp} - \beta_{imp})dx'\right\}} \tag{7.59}$$

The multiplication factor for the device can be defined by the relation

$$M_e = \frac{I}{i_e(0)} = \frac{i_e(W)}{i_e(0)} \tag{7.60}$$

i.e., the ratio of the electron current injected at $x = 0$ and the total current in the device. We get

$$M_e = \frac{i_e(0) + i_e(W) \int_0^W \beta_{imp} \; exp\left\{-\int_0^x (\alpha_{imp} - \beta_{imp})dx'\right\} dx}{i_e(0) \; exp\left\{-\int_0^W (\alpha_{imp} - \beta_{imp})dx\right\}} \tag{7.61}$$

Using standard solutions for the integral

$$exp\left\{-\int_0^W (\alpha_{imp} - \beta_{imp})dx\right\} = 1 - \int_0^W (\alpha_{imp} - \beta_{imp}) \; exp\left\{-\int_0^x (\alpha_{imp} - \beta_{imp})dx'\right\} dx \tag{7.62}$$

we get

$$M_e = \frac{1}{1 - \int_0^W \alpha_{imp} \; exp\{-\int_0^x (\alpha_{imp} - \beta_{imp})dx'\}dx} \tag{7.63}$$

The condition for breakdown is when $M_e \longrightarrow \infty$, i.e., when

$$\int_0^W \alpha_{imp} \; exp\{-\int_0^x (\alpha_{imp} - \beta_{imp})dx'\}dx = 1 \tag{7.64}$$

If the avalanche process is taking under a uniform electric field, the values of $\alpha_{imp}, \beta_{imp}$ have no spatial dependence and we have

$$M_e = \frac{1}{1 - \alpha_{imp} \int_0^W exp\{-(\alpha_{imp} - \beta_{imp})x\}dx}$$

$$M_e = \frac{1}{1 - \frac{\alpha_{imp}}{\alpha_{imp} - \beta_{imp}} [1 - exp\{-(\alpha_{imp} - \beta_{imp})W\}]} \tag{7.65}$$

If α_{imp} and β_{imp} are the same, we simply get

$$M_e \longrightarrow \frac{1}{1 - \alpha_{imp} W} \tag{7.66}$$

The values of M_e (or M_h) that can be obtained in real devices are limited by other processes that may occur at high fields, especially in narrow bandgap semiconductors. For example, tunneling current due to band to band tunneling limits M to ~10 in detection using $In_{0.53}Ga_{0.47}As$ material.

In an experimental setup, two factors related to circuit parameters limit the multiplication level reached. One is the series resistance R_s between the junction and the diode terminals. The second factor comes from the fact that once multiplication starts, the device temperature increases and this reduces α_{imp} and β_{imp} and thus limits $M_e(M_h)$. In a diode with a breakdown voltage V_B, the experimentally observed multiplication factor can be fitted to the following relation:

$$M = \frac{1}{\left[1 - \left(\frac{V - IR}{V_B}\right)\right]^n} \tag{7.67}$$

where n is a parameter depending upon the device design, R is an effective resistance which includes the series resistance R_S and any thermal effects, V is the applied bias.

7.7.2 APD Bandwidth

A key attraction of the APD's is the high gain that can be achieved in the device. Thus the device is suitable for detection of very low photon intensities. However, a price has to be paid in terms of the device bandwidth and noise. In an APD having the general configuration of Fig. 7.17, the device response is limited by three important times:

i) the transit time across the absorbing region

$$t_{tr}(e) = \frac{W_{abs}}{v_s(e)} \tag{7.68}$$

ii) the time required for the avalanche process to develop, t_A;

iii) the transit time for the holes generated during the avalanche process to transmit through the absorbing region back to the p-region.

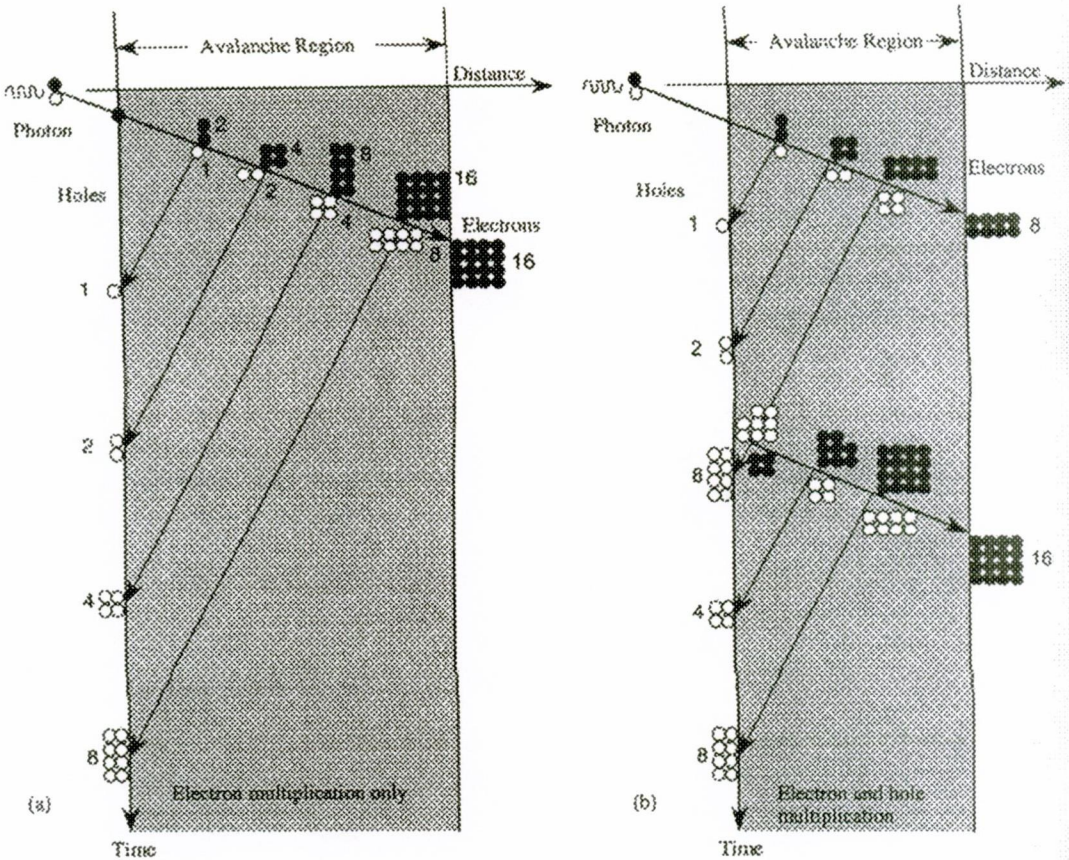

Figure 7.19. The avalanche build-up process shown as a function of time. (a) Only electrons are causing the carrier multiplication. (b) Both electrons and holes are causing the multiplication. (After J. Gowar, *Optical Communication Systems*, Prentice-Hall, Englewood Cliffs, New Jersey (1989).)

$$t_{tr}(h) = \frac{W_{abs}}{v_s(h)} \tag{7.69}$$

The avalanche delay time t_A depends upon the value of α_{imp}/β_{imp}. If $\alpha_{imp} \gg \beta_{imp}$, just a single pass of the electrons across W_{aval} generates the entire avalanche process as shown in Fig. 7.19. However, for a general α_{imp}/β_{imp} ratio, the delay time is

$$t_A = \frac{M\beta_{imp}W_{aval}}{\alpha_{imp}v_s(e)} \tag{7.70}$$

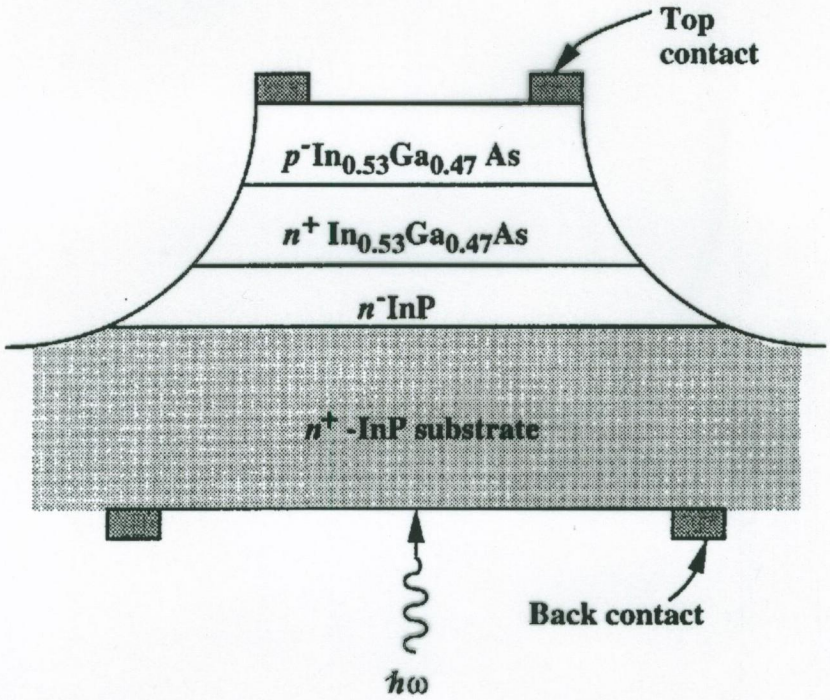

Figure 7.18: A schematic cross-section of a back illuminated InGaAs/InP avalanche photodiode. Due to the short absorption region, in the direct gap semiconductors, one can have the same region for absorption and avalanche processes.

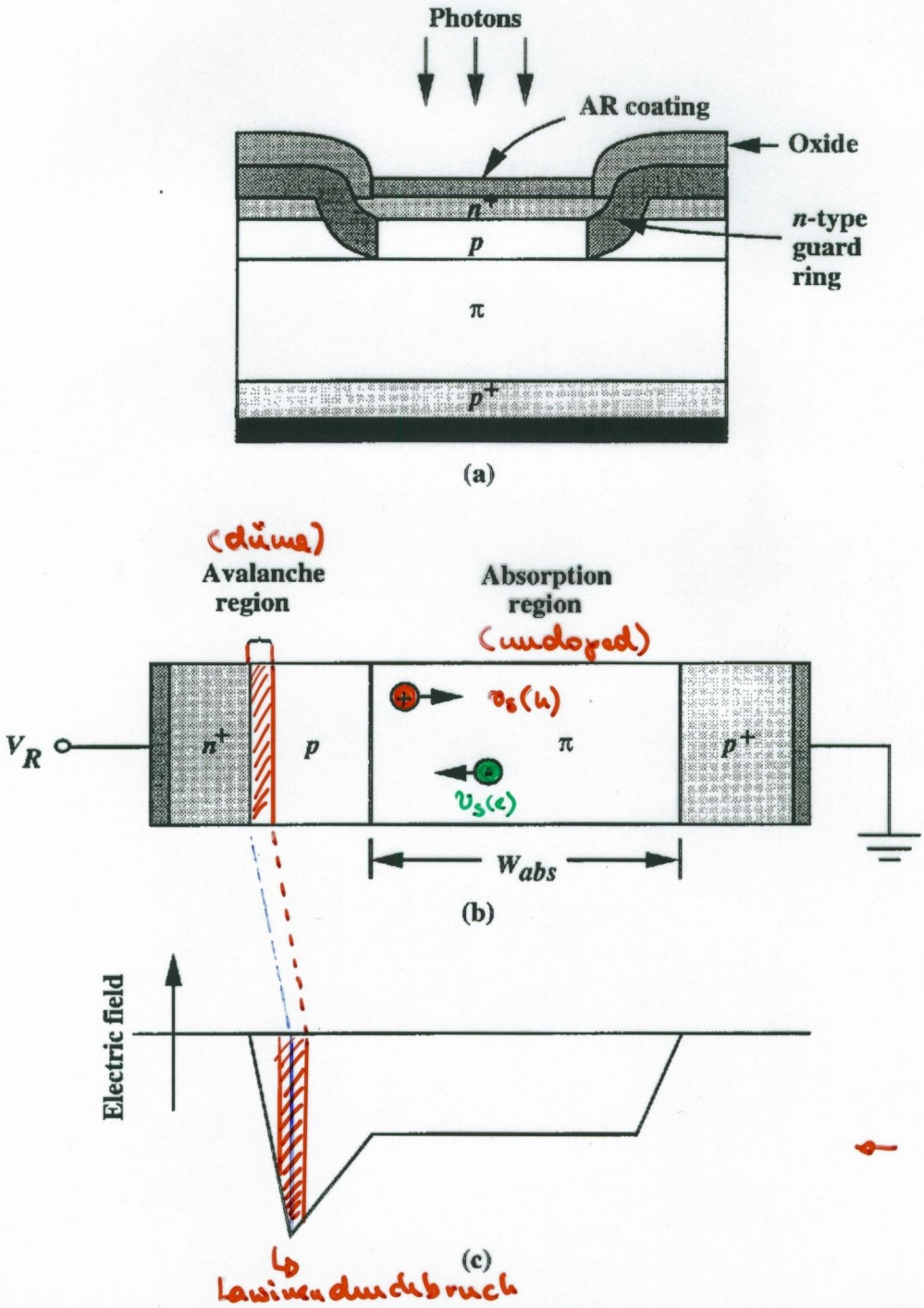

Figure 7.17: (a) A schematic of the reach through APD. (b) The cross-section of the APD showing the regions for absorption and avalanching. In the structure shown, the electrons are responsible for starting the multiplication process. (c) The electric field profile in the APD structure. The strong field at the n^+p junction causes the avalanche process.

$|\vec{E}| \geq 10^5$ V/cm

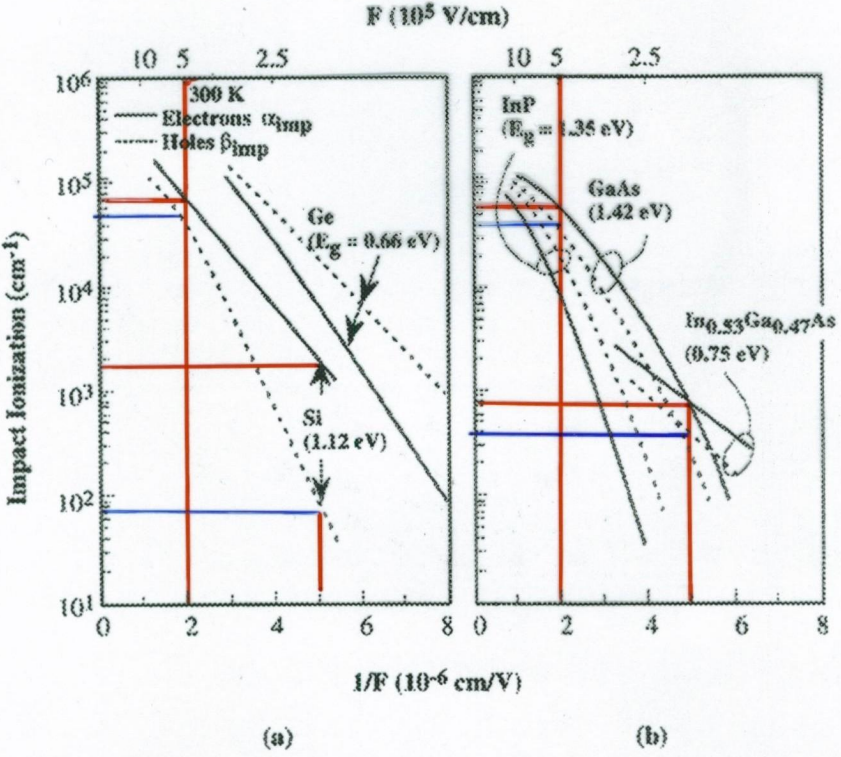

Figure B.3: Ionization rates for electrons and holes at 300 K versus reciprocal electric field for Ge, Si, GaAs, $In_{0.53}Ga_{0.47}$ and InP. (Si, Ge results are after S.M. Sze, *Physics of Semiconductor Devices*, John Wiley and Sons (1981); InP, GaAs, InGaAs results are after G. Stillman, *Properties of Lattice Matched and Strained Indium Gallium Arsenide*, ed. P. Bhattacharya, INSPEC, London (1993).

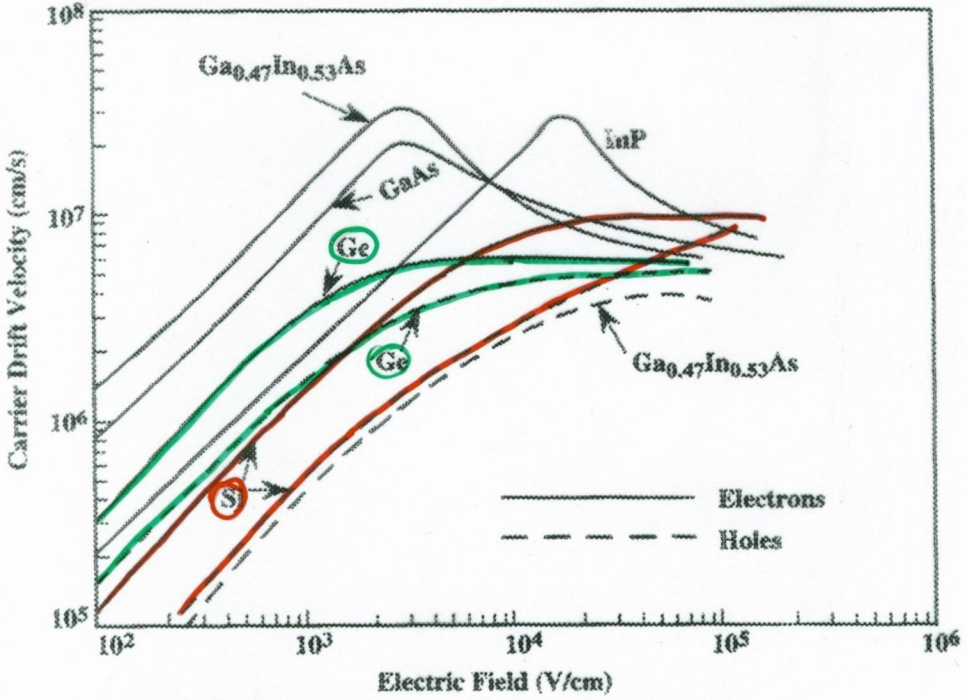

Figure B.2: Velocity-Field relations for several semiconductors at 300 K.

Lawinendurchbruchs detektor

(APJ - avalange process detector)

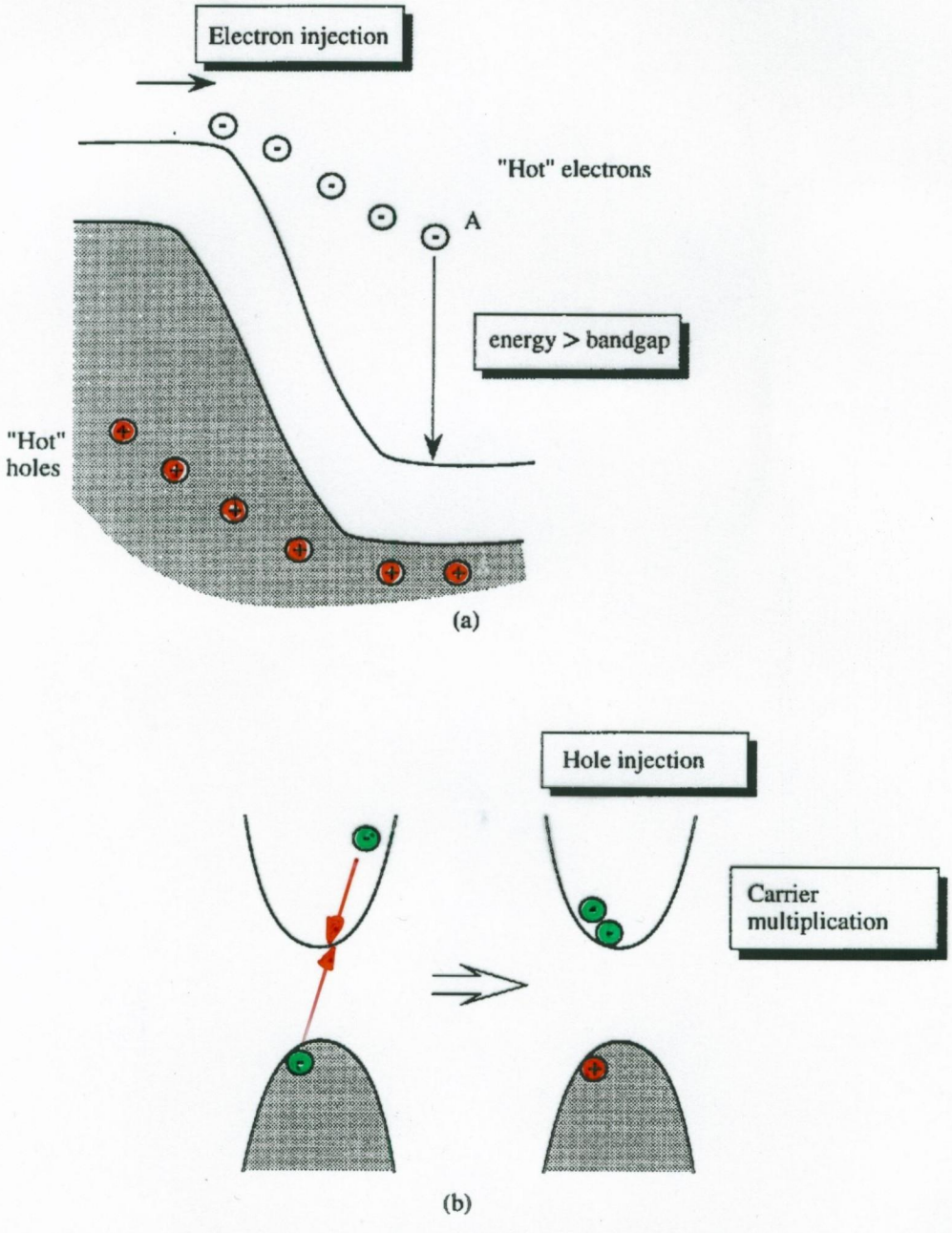

Figure 7.16: (a) A schematic of a reverse biased p-n junction. The electron A has an energy greater than the bandgap of the semiconductor. (b) A "hot" electron in the conduction band interacts with an electron in the valence band to generate two electrons and a hole, as shown.

Phototransistor

(n-p-n)

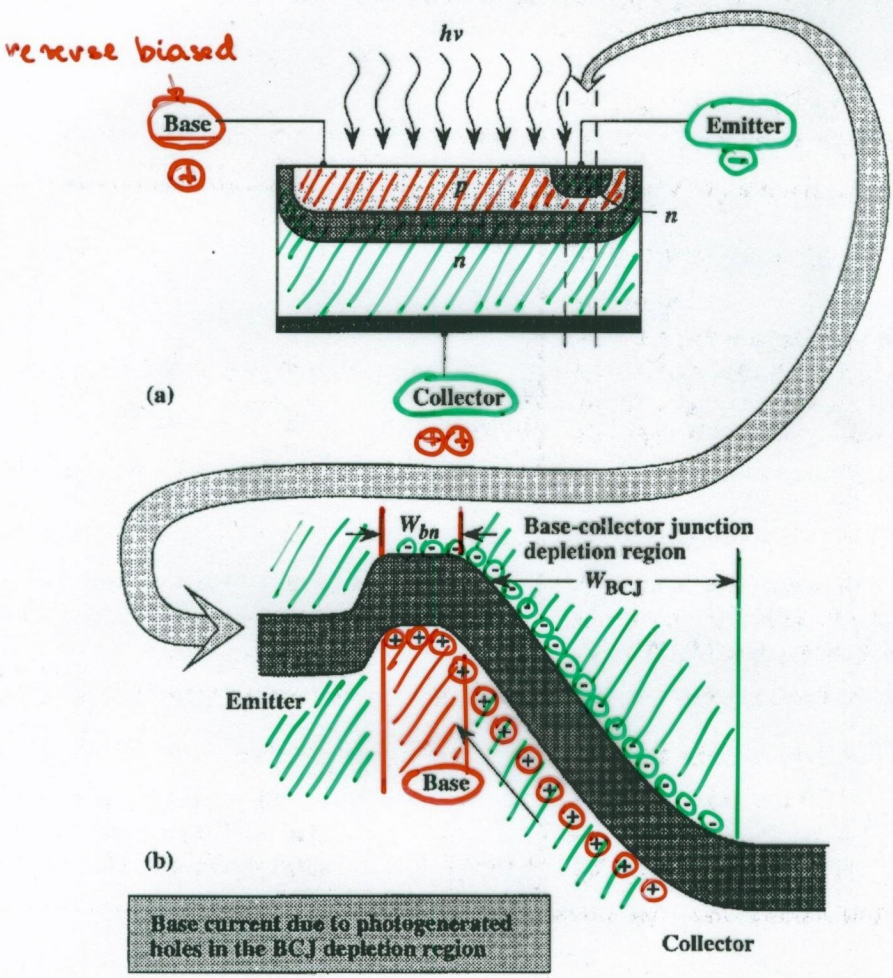

Figure 7.20: (a) A schematic of the phototransistor. (b) Band diagram of the phototransistor which is in the open base mode. Holes generated in the reverse biased base-collector junction region provide a base current signal which causes the electrons to be injected from the emitter.

E-B in forward direction

B-C in reverse bias